ACS OMEGA

Open Access

http://pubs.acs.org/journal/acsodf

Article

ZIKV Inhibitors Based on Pyrazolo[3,4-*d*]pyridazine-7-one Core: Rational Design, *In Vitro* Evaluation, and Theoretical Studies

Quang De Tran, Cuong Quoc Nguyen,* Quang Le Dang,* Thi Hong Minh Nguyen, Bui Thi Buu Hue, Minh Uyen Thi Le, Nguyen Trong Tuan, Nguyen Quoc Chau Thanh, Tran Thanh Men, Pham Minh Quan, Nguyen Duy Tuan, Thai Thi Cam, Nguyen Thi Thu Thuy, Vu Thi Bich Hau, Tran Duy Binh, and Hong Phuong Nguyen*

Cite This: *ACS Omega* 2023, 8, 48994−49008

Read Online

ACCESS | Metrics & More | Article Recommendations | Supporting Information

ABSTRACT: The Zika virus (ZIKV) is believed to cause birth defects, and no anti-ZIKV drugs have been approved by medical organizations to date. Starting from antimicrobial lead compounds with a pyrazolo[3,4-*d*]pyridazine-7-one scaffold, we synthesized 16 derivatives and screened their ability to interfere with ZIKV infection utilizing a cell-based phenotypic assay. Of these, five compounds showed significant inhibition of ZIKV with a selective index value greater than 4.6. In particular, compound **9b** showed the best anti-ZIKV activity with a selectivity index of 22.4 (half-maximal effective concentration = 25.6 μM and 50% cytotoxic concentration = 572.4 μM). Through the brine shrimp lethality bioassay, **9b**, **10b**, **12**, **17a**, and **19a** showed median lethal dose values in a range of 87.2−100.3 μg/mL. Compound **9b** was also targeted to the NS2B-NS3 protease of ZIKV using molecular docking protocols, in which it acted as a noncompetitive inhibitor and strongly bound to five key amino acids (His51, Asp75, Ser135, Ala132, Tyr161). Utilizing the pharmacophore model of **9b**, the top 20 hits were identified as prospective inhibitors of NS2B-NS3 protease, and six of them were confirmed for their stability with the protease via redocking and molecular dynamics simulations.

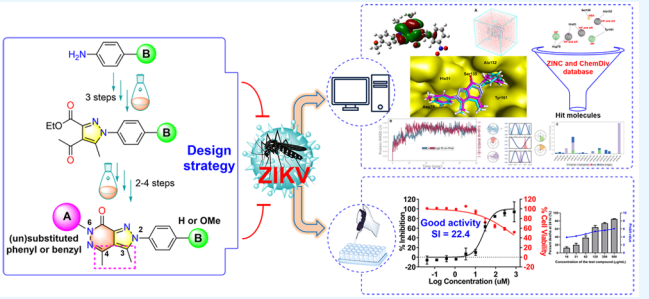

1. INTRODUCTION

ZIKV (Zika virus) is thought to cause birth defects as well as neurological problems.[1] Currently, there are no medicines or vaccines against ZIKV or specific antiviral treatments for clinical ZIKV infection.[1,2] Therefore, the development of new antivirus compounds that are effective, selective, and safe has been extremely necessary and urgent. In our previous research on bioactive heterocyclic compounds, berberine and benzimidazole derivatives were synthesized and exhibited a potential Zika antivirus with a selectivity index (SI) value greater than 10 and the half-maximal effective concentration (EC_{50}) of 1.9−48.3 μM.[3,4] In this study, we conducted works on heterocyclics and an assessment of their antiviral activity. It is found that bioorganic compounds containing heterocyclic amines (pyrazole or pyridazine) are particularly important in medicinal chemistry due to their diverse biological activities, and the relationships between their structures and pharmacological action have been studied for a long time.[5−8] The heterocyclic amines possess potential biological properties including antimicrobial, analgesic, anticancer, antifeeding, antitubercular, antidiabetic, antifungal, antihypertensive, antiplatelet, anticonvulsant, anti-HIV, antiasthma, anti-inflammatory, antipyretic, and insecticidal activities.[5−11] In particular, pyrazole-pyridazine compounds possess an extensive range of biological activities, and the fusion of pyrazole and pyridazine rings can give rise to five different bicyclic ring systems to help diversify and enhance the compound bioactivity (Figure 1A). For example, some pyrazolo-pyridazine derivatives showed antifungal[12] and insecticidal activities.[13] In medicinal chemistry, the pyrazolo-pyridazine compounds were also found to have anti-inflammatory[14] and anticancer properties.[7] These derivatives inhibited cyclin-dependent kinase,[13] glycogen synthase kinase 3 (GSK-3),[15] COX-2,[16] and fibroblast growth factor receptor (FGFR)[17] and were active against *Leishmania amazonensis* (Figure 1B).[18]

The types and preparations of the fused bicyclic ring structures such as pyrazolo[1,2-*a*]pyridazine, pyrazolo[3,4-*d*]pyridazinones, and pyrazolo[4,3-*c*]pyridazines have been reported by several synthesis methods.[19−24] These compounds have shown diversity and abundance of pharmacology,

Received: September 2, 2023
Revised: November 21, 2023
Accepted: November 27, 2023
Published: December 14, 2023

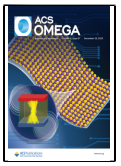

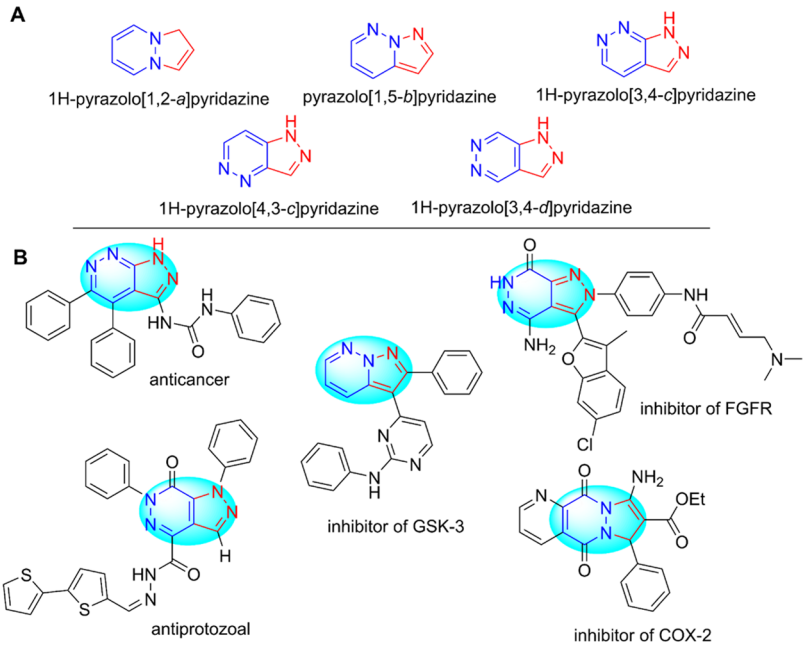

Figure 1. Pyrazolo-pyridazine structures with different ring fusion patterns (A) and representative compounds containing a pyrazolo-pyridazine unit (B).

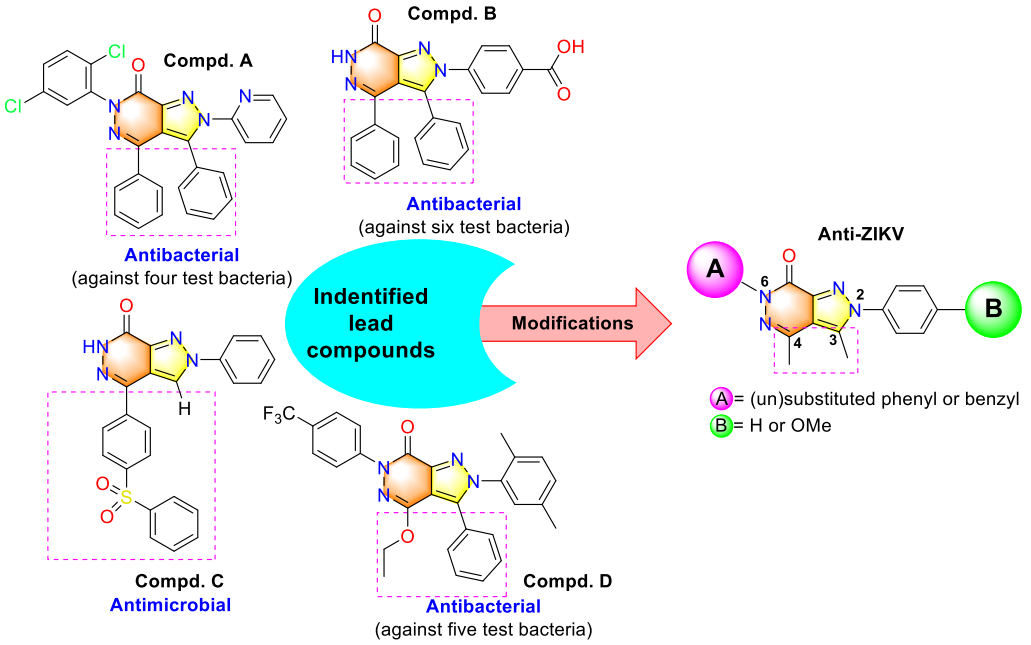

Figure 2. Rational design of the pyrazolo[3,4-*d*]pyridazin-7-one scaffold of lead compounds (A–D).

especially antibacterial and antimicrobial activities.[12,18,25,26] This also advocated an optimization of the synthesis of compounds containing the pyrazolo-pyridazine subunit with the repurposing of antiviral effects on ZIKV in this study. Zika virus NS2B-NS3 protease plays an essential role in viral replication.[27] The viral protease is therefore considered as an ideal antiviral compound target. To facilitate the development of novel viral inhibitors, we also aimed to search for effective ZIKV inhibitors targeting NS2B-NS3 protease from the pyrazolo[3,4-*d*]pyridazine-7-one core with superior potency and selectivity.

In the course of our research on the design and synthesis of heterocyclic compounds bearing functional groups at the pyrazolo[3,4-*d*]pyridazine-7-one core, we have set up a versatile organic synthetic process in the laboratory. Besides, the evaluation of anti-ZIKV activity of the synthesized compounds was also carried out. The *in vitro* results revealed that synthesized pyrazolo[3,4-*d*]pyridazine-7-one compounds exhibit highly potent activities against ZIKV. Furthermore, docking, molecular dynamics, and pharmacophore model experiments have also been approached and proposed for the NS2B-NS3 protease of ZIKV in this study.

2. RESULTS

2.1. Structural Design and Synthesis of Pyrazolo[3,4-*d*]pyridazine-7-one. In a series of previous studies, the

https://doi.org/10.1021/acsomega.3c06612
ACS Omega 2023, 8, 48994−49008

Scheme 1. General Procedure for the Synthesis of Compounds Containing the Pyrazolo[3,4-*d*]pyridazin-7-one Moiety[a]

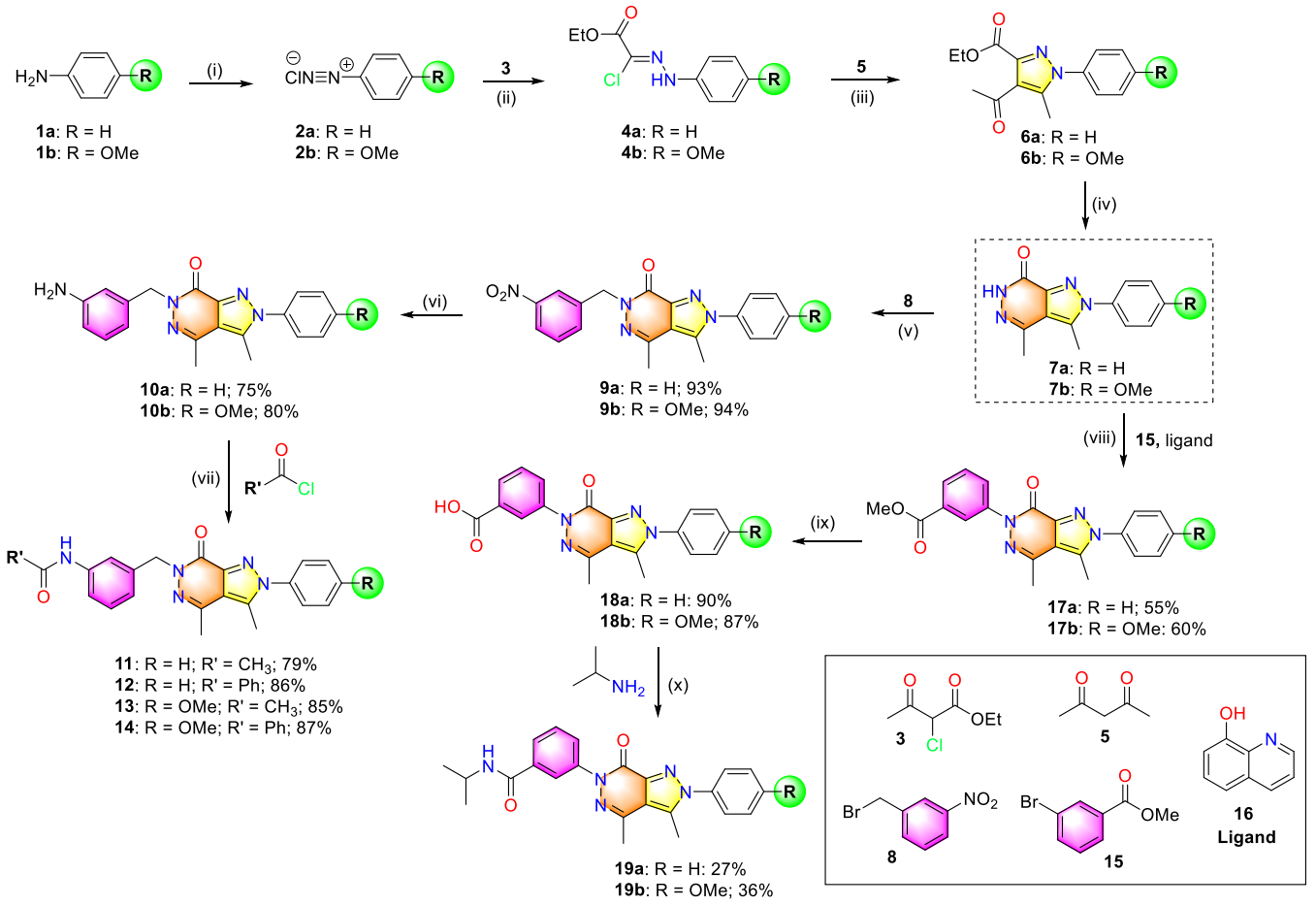

[a](i) Conc. HCl/H_2O (1:1), $NaNO_2/H_2O$, 0 °C, 1 h; (ii) EtOH, NaOAc, 0 °C, 1 h; (iii) NaOEt, EtOH, rt, 1 h; (iv) hydrazine hydrate, EtOH, reflux, 1 h; (v) DMF, NaH, 0 °C, 30 min; (vi) $SnCl_2 \cdot H_2O$, EtOH, reflux, 1 h; (vii) MC, TEA, 0 °C, 1 h; (viii) CuI, K_2CO_3, DMSO, microwave, 150 °C; (ix) LiOH 1 M, rt, overnight; (x) DMF, HOBT, EDC·HCl, rt, −50 °C, overnight.

pyrazolo[3,4-*d*]pyridazine-type compounds displayed effective antimicrobial and pharmacological properties (Figure 2).[12,18,19,23,25,26] In this study, pyrazolo[3,4-*d*]pyridazine-7-one core structures have been utilized as a lead core to prepare different compounds with a direction of antiviral activity enhancement. Figure 2 shows an approach that makes chemical modifications of known antibacterial pyrazolo-pyridazines with an expectation of the formation of antiviral activity. The series of pyrazolo[3,4-*d*]pyridazine-7-one core compounds was designed and emphasized points on molecular modulation specifically modifying different substituents of phenyl or benzyl at N^6 and their positions at N^2. Additionally, the design and synthesis of heterocyclic compounds that bear functional groups at the pyrazolo[3,4-*d*]pyridazine scaffold were performed by a versatile process in the laboratory (Scheme 1). We synthesized the pyrazolo[3,4-*d*]pyridazine-7-one scaffold (**7**) from aniline derivatives as shown in Scheme 1. First, benzenediazonium chloride **2** was obtained by diazotizing aniline with $NaNO_2$ in dilute HCl acid. In the next step, diazonium salt was used for the Japp-Klingemann reaction in situ by reacting with ethyl 2-chloroacetoacetate (**3**) to form an arylhydrazone.

Second, pyrazole-derived compound **6** bearing a carboxylate group and an acetyl group was prepared by condensation of an arylhydrazone with acetylacetone in the presence of NaOEt in ethanol. Third, the compound of 4-acetyl pyrazole **6** fairly readily reacted with hydrazine to produce pyrazolo[3,4-*d*]pyridazine-7-one scaffold (**7**) in high yield (>94%). A carefully detailed comparison of the spectral data recorded from compound **7a** with compound **7b** has shown their carbon skeleton similarity. The main differences in structure between **7a** and **7b** were the appearance of a methoxy group [δ_H 3.82 (*s*, 3H)] in the benzene moiety of **7b**. The ^{1}H NMR spectrum of compound **7a** indicated the −NH− moiety of pyrazolo[3,4-*d*]pyridazine scaffold at δ_H 12.03 (*s*, 1H), N^2-substituted phenyl moiety at δ_H 7.62 (*s*, 5H), and two methyl groups were attached to heterocyclic at C^4 and C^3 (δ_H 2.49, δ_H 2.60, respectively). In the ^{1}H NMR spectrum of compound **7b**, the signal at δ_H 11.96 indicated the −NH− moiety and the signals of two methyl groups revealed at 2.54 (*s*, 3H) and 2.45 (*s*, 3H). The N^2-substituted aromatic ring system signals were observed at δ_H 7.12 (2H, *d*) and 7.49 (2H, *d*) (Supporting Information, Figures S1−S4).

Compound **7** was utilized as the raw material for synthesizing other compounds substituted for the benzyl group at the N^6 site (Scheme 1). Compound **9** was obtained by a nucleophilic substitution reaction of **7** with 3-nitrobenzyl bromide in dimethylformamide (DMF). The nucleophilic substitution reaction between the pyrazolo-pyridazine derivative **7** and 3-nitrobenzyl bromide in DMF medium is very

https://doi.org/10.1021/acsomega.3c06612
ACS Omega 2023, 8, 48994−49008

readily generating compound **9** in high yield (>93%). In the next step, the nitro group was converted to amine **10** by a reduction process using the reducing agent tin(II) chloride monohydrate in ethanol under reflux conditions. The amine functional group was coupled with acid chloride to form amides **11** to **14**, respectively. They were prepared by the presence of triethanolamine (TEA) in methylene chloride (MC) at 0 °C, with good yields (>79%). Starting from the core structure of **7**, the copper-catalyzed coupling reaction of aryl halide compound with nitrogen-containing nucleophile was applied for the synthesis of **17** by coupling between **7** and methyl 3-bromobenzoate (**15**) in the presence of CuI catalyst, K_2CO_3, dimethyl sulfoxide (DMSO), and 8-hydroxyquinoline ligand (**16**) under microwave conditions (yields of 55 to 60%). In the next steps, including ester group hydrolysis using LiOH and HCl, **18** was obtained with good yields (>87%). Finally, treatment of **18** with propane-2-amine gave the desired pyrazolo-pyridazinone **19** (yields of 27 to 36%). The carbodiimide 1-ethyl-3-(3-(dimethylamino)propyl)-carbodiimide (EDC) was used for solution-phase peptide couplings as its urea byproduct could be removed by washing in an aqueous workup. After the completion of the reaction, the products were purified by silica gel column chromatography and characterized by NMR and high-resolution mass spectrometry (HR-MS). Some synthesized compounds were also subjected to high-performance liquid chromatography (HPLC) and gas chromatography−flame ionization detector (GC-FID) analyses to test their purity. As a result, the selected compounds had a purity of more than 95% based on the area percentage (Supporting Information, Figures S5−S27).

2.2. Anti-ZIKV Activity of the Synthesized Pyrazolo-[3,4-*d*]pyridazine-7-one. The present study aims to evaluate the antiviral activity of 16 pyrazolo[3,4-*d*]pyridazine-7-one compounds against the Zika virus strain MR766 of the Africa lineage, while also assessing their potential cytotoxic effects on Vero cells. Mycophenolic acid (MPA), an immunosuppressant, was used as a positive control.[3,4] The African lineage strain ZIKV-MR766 was incubated with the compounds for 24 h prior to the Vero cell infection through the viral immunofluorescence assay; the results of anti-ZIKV bioassay are presented in Table 1, and the dose−response curves of the top five compounds were displayed in Figure 3. Five compounds (**9b**, **10b**, **12**, **17a**, and **19a**) showed activity against ZIKV with a selective index value greater than 4 (SI > 4), while the other nine compounds showed little to no effects on ZIKV (SI < 4). In particular, compound **9b** exhibited a strong anti-ZIKV efficacy with an SI value of 22.4 (EC_{50} = 25.6 μM and 50% cytotoxic concentration (CC_{50}) = 572.4 μM), and a potency of 2.6-fold to 4.6-fold than those of the other compounds. Two compounds (**10b** and **12**) showed moderate activities with SI values greater than 6.9 (EC_{50} = 144.3 μM and 140.1 μM; CC_{50} ≥ 1000 μM and >1000 μM, respectively). Nevertheless, compounds **17a** and **19a** were weakly active against ZIKV (SI > 4.6) (EC_{50} = 218.1 and 87.2 μM; and CC_{50} ≥ 1000 and 435.6 μM, respectively).

In addition, a cytotoxicity assay was conducted to determine their 50% cytotoxicity concentration (CC_{50}) against virus-uninfected Vero cells. The results revealed that **7a**, **9b**, **10b**, **11**−**14**, **17a**, **17b**, **18a**, **19a**, and **19b** exhibit low cytotoxicity, with CC_{50} values greater than 240 μM (Table 1). Furthermore, at a concentration of 10 μM, all of the test compounds maintained 90% of Vero cell viability. Notably, six compounds (**7a**, **9b**, **10b**, **12**, **14**, **17a**, and **18a**) displayed low cytotoxicity with CC_{50} values higher than 500 μM (Supporting Information, Table S1).

Table 1. ZIKV Inhibitory Activity of the Synthesized Pyrazolo[3,4-*d*]pyridazine-7-ones against Zika Virus Strain MR766

Compd.	EC_{50}[a] (μM)	CC_{50}[b] (μM)	SI[c]
7a	697.5 ± 4.9	2606 ± 4.9	3.7
7b	39.1 ± 1.8	114.6 ± 7.5	2.9
9a	ND[e]	ND	NA[f]
9b	25.6 ± 2.8	572.4 ± 5.1	22.4
10a	ND	ND	NA
10b	144.3 ± 3.9	>1000	>6.9
11	203.6 ± 3.2	361 ± 1.9	1.8
12	140.1 ± 13.7	>1000	>7.1
13	124.3 ± 4.6	245.4 ± 10.3	2.1
14	300.3 ± 6.5	>1000	>3.3
17a	218.1 ± 3.8	>1000	>4.6
17b	161.3 ± 9.1	368.5 ± 4.2	2.3
18a	>1000	>1000	NA
18b	ND	ND	NA
19a	87.2 ± 7.3	435.6 ± 2.8	5.0
19b	105.0 ± 4.6	299.8 ± 8.3	2.9
MPA[d]	0.94	>1000	>1063

[a]EC_{50}: median effective concentration. [b]CC_{50}: 50% cytotoxic concentrations. [c]SI: Selectivity index (CC_{50}/EC_{50}). [d]MPA: mycophenolic acid (positive control). [e]ND: not determined. [f]NA: not applicable (compounds were tested, but CC_{50} and EC_{50} values could not be calculated). EC_{50} and CC_{50} values were calculated by analysis of 10-point dose−response curves in triplicate.

2.3. Toxicity Bioassay. One of the biggest concerns during the drug discovery process is the toxicity of the components, and any undesirable toxicity must be carefully monitored. Thus, in this study, we evaluated the toxicity of the compounds that have the highest anti-ZIKV efficacy by a brine shrimp lethality bioassay. The brine shrimp (*Artemia salina*) lethality assay was conducted on five compounds with strong anti-ZIKV efficacy (**9b**, **10b**, **12**, **17a**, and **19a**). Toxicity test results are presented in Table 2. The result is the lethality of compounds on brine shrimp with estimated median lethal dose (LD_{50}) values that range from about 87.2 to 114.1 μg/mL. The tested compounds also showed concentration-dependent toxicity against brine shrimp. Besides, at concentrations greater than 500 μg/mL, all nauplii mortalities were higher than 80%. In particular, we found that these compounds have considerably lower toxicity than a berberine derivative, which was previously reported to be a ZIKV inhibitor[4] (Supporting Information, Figure S28). Based on the toxicity index, these compounds were considered to be moderately toxic, indicating that they could be extended for further preclinical studies.

2.4. Docking Protocol. To study the interactions between ZIKV NS2B-NS3 protease (5H4I) and compounds **9b** (most active) and **17a** (least active), the Autodock program was used in a molecular docking study similar to docked berberine derivatives in our previous study.[4] A comprehensive analysis of molecular interactions, hydrogen bonds, and hydrophobic interactions, particularly within the active site of the NS2B-NS3 protease, was performed for the selected compounds (Figure 4). The binding energies of both **9b** and **7a** were lower than those of the cocrystallized ligand (benzimidazole-1-ylmethanol), thus showing better binding affinity and stability than this ligand (−8.16, −7.60, and −6.53 kcal/mol,

https://doi.org/10.1021/acsomega.3c06612
ACS Omega 2023, 8, 48994−49008

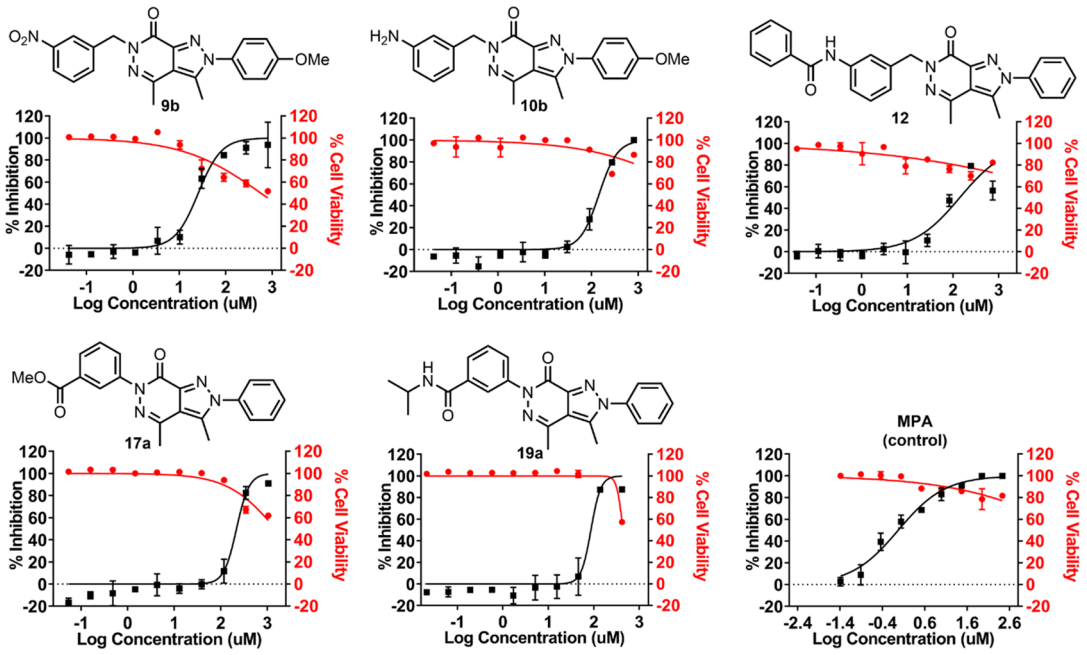

Figure 3. Dose−response curves of compounds **9b**, **10b**, **12**, **17a**, and **19a** against ZIKV and the reference inhibitor (MPA-mycophenolate acid). The percentage of ZIKV inhibition is shown in the black line. Percentage cell viability is shown in the red line. A compound shows good activity if the SI value is greater than 10 (SI of 10−6: activity; SI of 6−4: low activity; and SI < 4: no activity). A full antiviral data set for all compounds can be found in the Supporting Information, Table S1.

Table 2. Toxicity of the Selected Pyrazolo[3,4-*d*]pyridazine-7-one from Brine Shrimp Assay

Compd.	LD_{50} (μg/mL)[a]	95% fiducial limits	
		Lower	Upper
9b	91.7	**67.2**	**124.9**
10b	100.3	**77.3**	**130.1**
12	114.1	**88.4**	**147.3**
17a	87.2	**65.5**	**115.9**
19a	90.3	**64.5**	**126.5**
Atropine SO_4[b]	737.8	**477.4**	**>1000**
Berberine chloride[b]	27.0	21.5	33.8
ref. inhibitor[c]	34.6	27.9	42.8

[a]LD_{50}: median lethal dose (μg/mL). LD values were estimated by probit analysis of 6-point dose (16−500 μg/mL). [b]Atropine sulfate monohydrate and berberine chloride were used as the positive controls. The solvent was used as the negative control (lower than 1% DMSO). [c]The ZIKV inhibitor (berberine derivative-**4d**) was described in our previous report, and it was also used as a standard.[4]

respectively) (Supporting Information, Figure S30). The benzyl function at N^6 showed a more favorable orientation than the phenyl function in the hydrophobic region of the active site. This makes the aromatic ring of **9b** sandwiched between the side chains of Ala132-Tyr161 with a distance shorter than that of **17b** (3.58 and 4.35 Å for Ala132, and 5.35 and 5.40 Å for Tyr161, respectively). Compound **9b** also showed a distance with Ser135 shorter than that of **17a** (3.09 Å versus 3.54 Å, respectively) (Supporting Information, Figure S30). This may be the reason that **17b** was less active than **9b**. The substituted phenyl moieties (B) at N^2 were found in the hydrophobic pocket and sandwiched with Asp75 and Asp83 (pi-anion). Both pi-pi-stacked and pi-pi T-shaped bonds were observed between the pyrazolo[3,4-*d*]pyridazine-7-one scaffold and His51 with a distance of about 4.25 to 5.33 Å. Additionally, **9b** caused interactions with some key amino acids such as Thr134 (carbon−hydrogen bond), Gly151 (carbon−hydrogen bond), Trp50 (pialkyl), and Val72 (carbon−hydrogen bond). Compound **17a** also displayed interactions with some amino acids (Tyr150 and Tyr130) in the binding pocket.

2.5. Molecular Dynamic Simulation Study. A molecular dynamics simulation study was also performed to check the stability of the **9b**-NS2B-NS3 complex during 50000 ps (or 50 ns) based on the molecular docking results (Figure 5A). The root-mean-square deviation (RMSD) plot indicated that the **9b**-NS2B-NS3 complex reached its stable form after 10000 ps (or 10 ns), where the ligand is still intact with protein and not diffused away easily (Figure 5B). In addition, the molecular dynamic results displayed favored hydrophobic interactions with Tyr161 (94%), Phe84 (24%), and His51 (27%), hydrogen interaction with Ser135, and water-bridged interactions with Gly151 and Asn152 (Figure 5C). Figure 5D,E presents a ligand torsion histogram illustrating the dynamic changes in each rotatable bond throughout the simulation trajectory. These findings offer valuable insights into the conformational strain that preserves the ligand's shape when bound to the protein.

2.6. HOMO and LUMO Analysis. The properties of the highest occupied molecular orbitals (HOMOs) and lowest unoccupied molecular orbitals (LUMOs) hold significant utility for chemists. Molecules characterized by higher HOMO values and lower LUMO values are prone to facile oxidation and reduction, respectively. Illustrated in Figure 6 are the HOMO and LUMO surfaces, revealing a concentration of HOMO orbitals primarily around the pyrazolo[3,4-*d*]-pyridazine-7-one core. In both gas and water phases, compound **9b** exhibits HOMO−LUMO energy gaps of 7.75 and 7.62 eV, respectively. These energy parameters signify the molecule's remarkable stability and chemical hardness.

https://doi.org/10.1021/acsomega.3c06612
ACS Omega 2023, 8, 48994−49008

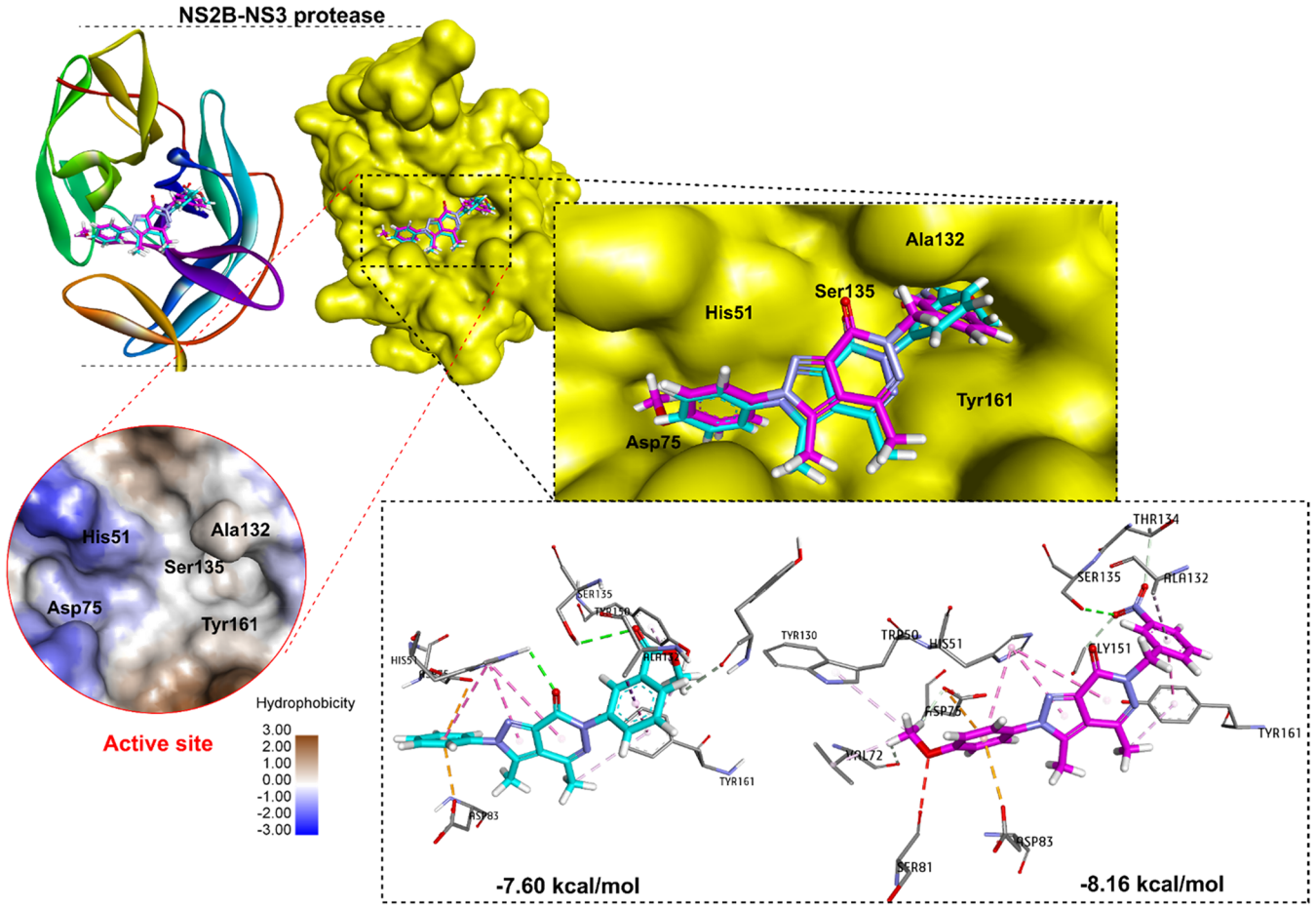

Figure 4. Binding interaction between **9b** (pink) and **17b** (cyan) at the active site of NS2B-NS3.

2.7. Pharmacophore Model and Pharmacophore-Based Virtual Screening. To identify important pharmacological features necessary for the screening of promising ZIKV inhibitors, we have implemented pharmacological modeling based on the structure of NS2B-NS3 docked to inhibitor **9b** using Pharmit online[28] by loading the docked features. First, Pharmit identified 13 pharmacological features from compound **9b** based on ligand−protease interactions (Figure 7A). Six sites involved in the interaction with key amino acids at the active site of NS2B-NS3 were selected to create a pharmacological model (Figure 7B). The pharmacophore model was chosen to contain one hydrogen acceptor from the hydroxyl group of Ser135, two hydrophobic regions engaging with Asp75 and Tyr161, and three featuring aromatic/hydrophobic regions interacting with His51 and Ala132. This pharmacophore model served for the virtual screening of compounds from databases or to optimize the modifications of lead compounds or inhibitors to obtain greater inhibitory efficacy. Two large databases, ZINC and ChemDiv, were used for virtual screening based on pharmacophore models in the present work. The ZINC database, containing more than 13 million molecules, yielded 1394 compounds that fit the model (RMSD < 1.0 Å) following screening, among which 536 molecules complied with Lipinski's rule of five. Similarly, screening from the ChemDiv database (over 1 million molecules) resulted in 807 compounds that fit the model, among which 303 molecules followed Lipinski's rule of five (Figure 7C). The two compounds ZINC1064562 (RMSD = 0.430 Å) and ChemDiv-L856−0019 (RMSD = 0.438 Å) exhibited the highest similarity to the model and were predicted to interact strongly with NS2B-NS3 protease, similar to compound **9b** (Supporting Information, Table S2). The screened top three compounds of each database were used to perform molecular docking and molecular dynamic processes (Figure 8). Based on the results, it can be inferred that the six chosen compounds exhibit a favorable binding energy with the NS2-NS3 protease, as their predicted binding energies are lower than −6.9 kcal/mol. Notably, compound ChemDiv-L856−0019 displays even lower energies than **9b** (−9.4 and −8.13 kcal/mol, respectively). Moreover, the stability of the ligand−receptor complex was assessed via molecular dynamics simulations over a period of 50 ns. The results indicate that the compounds maintain stability throughout the simulation; the RMSD values obtained were less than 4 Å. In summary, this investigation contributed to expanding the collection of compounds with the potential to effectively inhibit Zika virus.

3. DISCUSSION

In this study, 16 pyrazolo[3,4-*d*]pyridazine-7-one compounds were rationally designed and tested against the Zika virus (MR766 Africa lineage). We also assessed their cytotoxicity in Vero cells. In a previous patent, pyrazolo-pyridazone compounds were found to inhibit hepatitis C virus (HCV) at concentrations ranging from 0.01 to 3.06 μM.[29,30] Both hepatitis C virus and ZIKV belong to the genus Flavivirus and the family Flaviviridae. In our previous study, we also

https://doi.org/10.1021/acsomega.3c06612
ACS Omega 2023, 8, 48994−49008

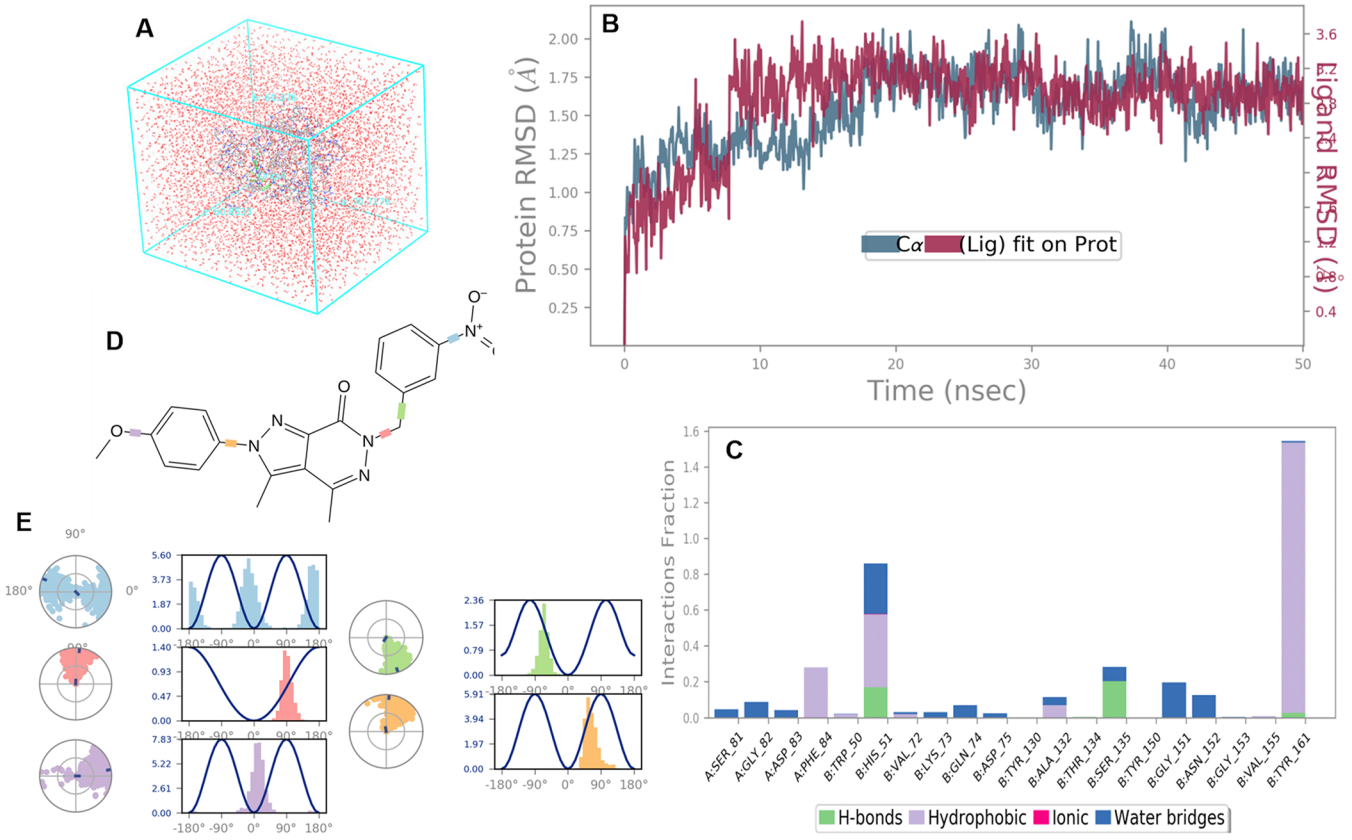

Figure 5. Molecular dynamics result for the **9b**-NS2B-NS3 complex. (A) Protein at the center of the water box in simulation protocol using Desmond Academic license 2018−4. (B) The RMSD values for complex during the molecular dynamic simulation. (C) Protein interactions with the ligand **9b** (hydrogen bonds, green; hydrophobic, violet; ionic, pink; and water bridges-blue). (D) Ligand torsion profile torsion and flexibility. (E) Ligand torsion angles.

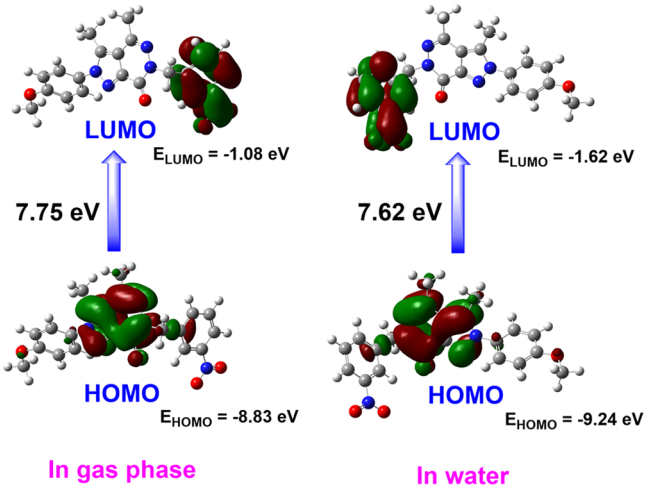

Figure 6. HOMO and LUMO orbitals of compound **9b** in the gas phase and water.

discovered benzimidazole derivatives as promising antiviral candidates for ZIKV treatment.[3] Seven benzimidazole derivatives strongly inhibited the African ZIKV strain with EC_{50} values lower than 13 μM. In particular, these compounds all showed resistance to the HCV virus with a selectivity index (SI) greater than 3.5. Therefore, we hypothesized that pyrazolo-pyridazone compounds will have the potential for ZIKV inhibition. The pyrazolo[3,4-*d*]pyridazine compounds also displayed an effective antiviral activity against rotavirus Wa strain and adenovirus type 7.[31] According to Akbas and Berbe,[12] compound A, one of seven new pyrazolo[3,4-*d*]pyridazine-7-one derivatives that was prepared via a furandione derivative, had the highest antibacterial activity against Gram-negative and Gram-positive bacteria (four test bacteria) with MICs (minimum inhibitory concentrations) in the range of 0.31 to <0.0024 mg/mL. Besides, lead compound B was synthesized from reactions of pyrazole-3-carboxylic acid with some hydrazine compounds, which also showed inhibitory activity against six test bacteria, including *Escherichia coli*, *Bacillus subtilis*, *Pseudomonas aeruginosa*, *Klebsiella pneumonia*, *Proteus vulgaris*, and *Xanthomonas compestris*.[19] In 2016, Mady et al. synthesized compound C, a pyrazolo[3,4-*d*]pyridazine-7-one linked to a diaryl sulfone moiety by using microwave irradiation; this compound also had effects on pathological bacterial strains such as *E. coli* O157 and *S. typhimurium*.[25] Compound D displayed antibacterial activity against five bacteria owing to containing a pyrazole-pyridazine subunit, which was also stronger than those of the positive controls by Erythromycin, Rifampicin, and Amikacin.[23] Based on the above-mentioned data, we designed a facile methodology for the design of pyrazolo[3,4-*d*]pyridazine-7-one linked to the methyl moiety at C^3 and C^4 from the original pyrazolo[3,4-*d*]pyridazine scaffold. The N^2 and N^6 positions of the pyrazolo[3,4-*d*]pyridazine-7-one core were introduced with benzyl or phenyl groups to form the respective compounds (Scheme 1 and Figure 2).

Sixteen compounds were synthesized, and then *in vitro* antiviral experiments were conducted to evaluate anti-ZIKV

https://doi.org/10.1021/acsomega.3c06612
ACS Omega 2023, 8, 48994−49008

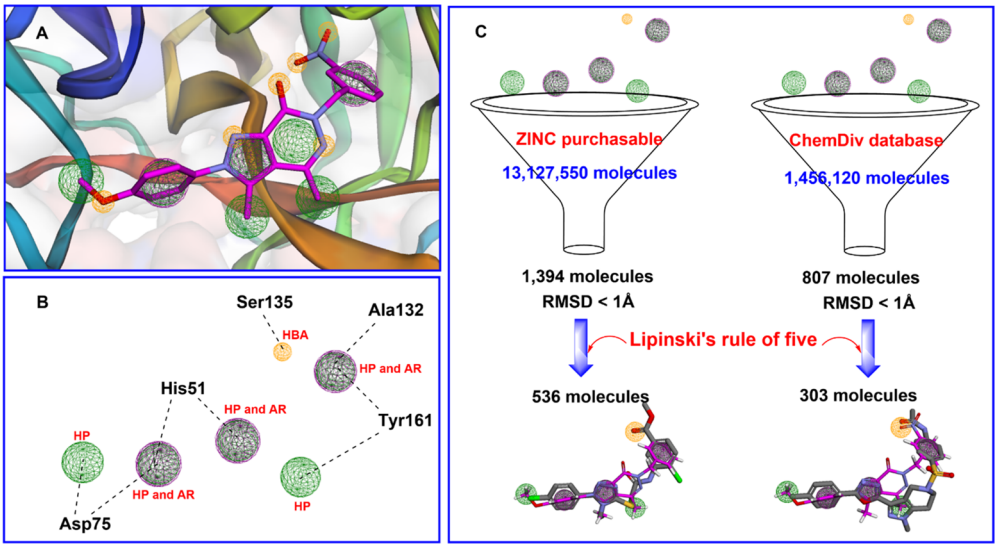

Figure 7. Pharmacophore model. (A) Pharmacophoric features of **9b** (pink) at the active site of the NS2B-NS3 protease. (B) Pharmacophoric features of **9b** were selected at the active site of NS2B-NS3 protease. (C) Pharmacophore-based virtual screening from the ZINC and ChemDiv database. HBA (hydrogen bond acceptor-organ sphere). HP (hydrophobic areas-green sphere). AR (aromatic ring-violet sphere).

activity. The docking study, molecular dynamics, and pharmacophore model of the highly active compounds were also carried out subsequently. It is noteworthy that compound **9b** was observed to be a potential new ZIKV inhibitor with an EC_{50} of 25.6 μM and a selectivity index value of greater than 22. In addition, compounds **10b**, **12**, **17a**, and **19a** also exhibited strong activity against Zika virus strain MR766 with SI values of 5.0 to >6.9 (Table 1 and Figure 3).

The brine shrimp lethality assay is a quick and simple biological test to estimate the lethal dose (LD) of purified compounds or plant extracts. Several studies suggest that these experiments are reasonably correlated with cytotoxic and antitumor properties.[32−34] Berberine chloride and atropine sulfate were used as standard drugs in cytotoxicity activity. Berberine is relatively toxic parenterally and has been used orally with potential antineoplastic, radiosensitizing, anti-inflammatory, antilipidemic, and antidiabetic activities.[35,36] Atropine was included in the World Health Organization's list of Essential Medicines, which can be administered by intravenous, subcutaneous, intramuscular, intraosseous, oral, endotracheal, and ophthalmic methods.[37] After 24 h of assessment, all the brine shrimp survived in the negative controls. In the positive controls treated with berberine, all the nauplii were dead at 125 μg/mL and the LD_{50} value was 27.0 μg/mL. In contrast, atropine sulfate showed mortality below 20% after 24 h (LD_{50} = 737.8 μg/mL) (Table 2 and Supporting Information, Figure S28). The brine shrimp's bioassay for the lethality of selected compounds (**9b**, **10b**, **12**, **17a**, and **19a**) resulted in their LD_{50} values of 91.7, 100.3, 114.1, 87.2, and 90.3 μg/mL, respectively. Compared with our previously reported ZIKV inhibitors, the evaluated compounds possessed lower toxicity than those of the berberine derivatives (LD_{50} = 34.6 μg/mL).[4] Therefore, the compounds in this study showed an acceptable toxicity range and could be candidates for the development of oral antiviral drugs and may have the potential to inhibit several cancer cell lines.

NS2B-NS3 protease plays a crucial role in the ZIKV activity due to it being responsible for site-specific cleavage of precursor polyprotein in ZIKV, and NS2B acts as a cofactor for NS2B-NS3 protease activation.[38] Special, several NS2B-NS3 inhibitors were identified as bromocriptine (IC_{50} = 21.6 μM), novobiocin (IC_{50} = 14.2 μM), temoporfin (IC_{50} = 1.1 μM), and erythrosine B (IC_{50} = 1.7 μM).[39−41] Choudhry et al. recently selected seven antiviral drug candidates, which were targeted to target NS2B-NS3 protease, using GOLD and AutoDock Vina software.[39] Thirumoorthy et al. screened and identified three potential compounds derived from Andrographis paniculate for ZIKV inhibition by targeting NS2B-NS3.[42] Therefore, NS2B-NS3 is the prioritized target for research in screening potential inhibitors against the Zika virus. In a recent work by us, a designed and synthesized berberine derivative was reported to be a potent inhibitor of Zika virus MR766 Africa lineage with an IC_{50} value of 5.3 μM and SI value of 15.3.[4] This derivative caused a high affinity for binding to the NS2B-NS3 protease, which suggests a potential for its protease inhibition in the future. Using a virtual screening model to partially predict experimental results seemed to be the simplest and best option. First, the redocking was done with the reference ligand (cocrystallized ligand) into the active site of NS2B-NS3 to protocol authentication (Supporting Information, Figure S29) before we performed molecular docking for two selected compounds (**9b** and **17a**). The obtained results displayed that the docked ligand completely overlapped with the cocrystallized ligand in protease root-mean-square deviation (RMSD value was 0.5936 Å). At the binding site, the docked ligand displayed interactions with some key amino acids as found in the crystal structure in the original PDB (5H4I).

The inhibitors' binding mode with protease was previously reported, and His51, Asp75, and Ser135 were key amino acids that participated in H-bond and hydrophobic interactions.[43,44] Especially, Ser135 played a vital role in the inhibition activity of the compound with this target enzyme. The benzimidazole ring of the cocrystallization ligand was sandwiched between the side chains of Ala132-Tyr161, so both of these amino acids were considered key residues.[45] The docking protocol showed that both compounds interact with the key amino acids at the active site of NS2B-NS3 protease with binding energies lower than −7.6 kcal/mol. The **9b**-NS2B-NS3 complex formed a catalytic triad at the active site characterized by the presence of

https://doi.org/10.1021/acsomega.3c06612
ACS Omega 2023, 8, 48994−49008

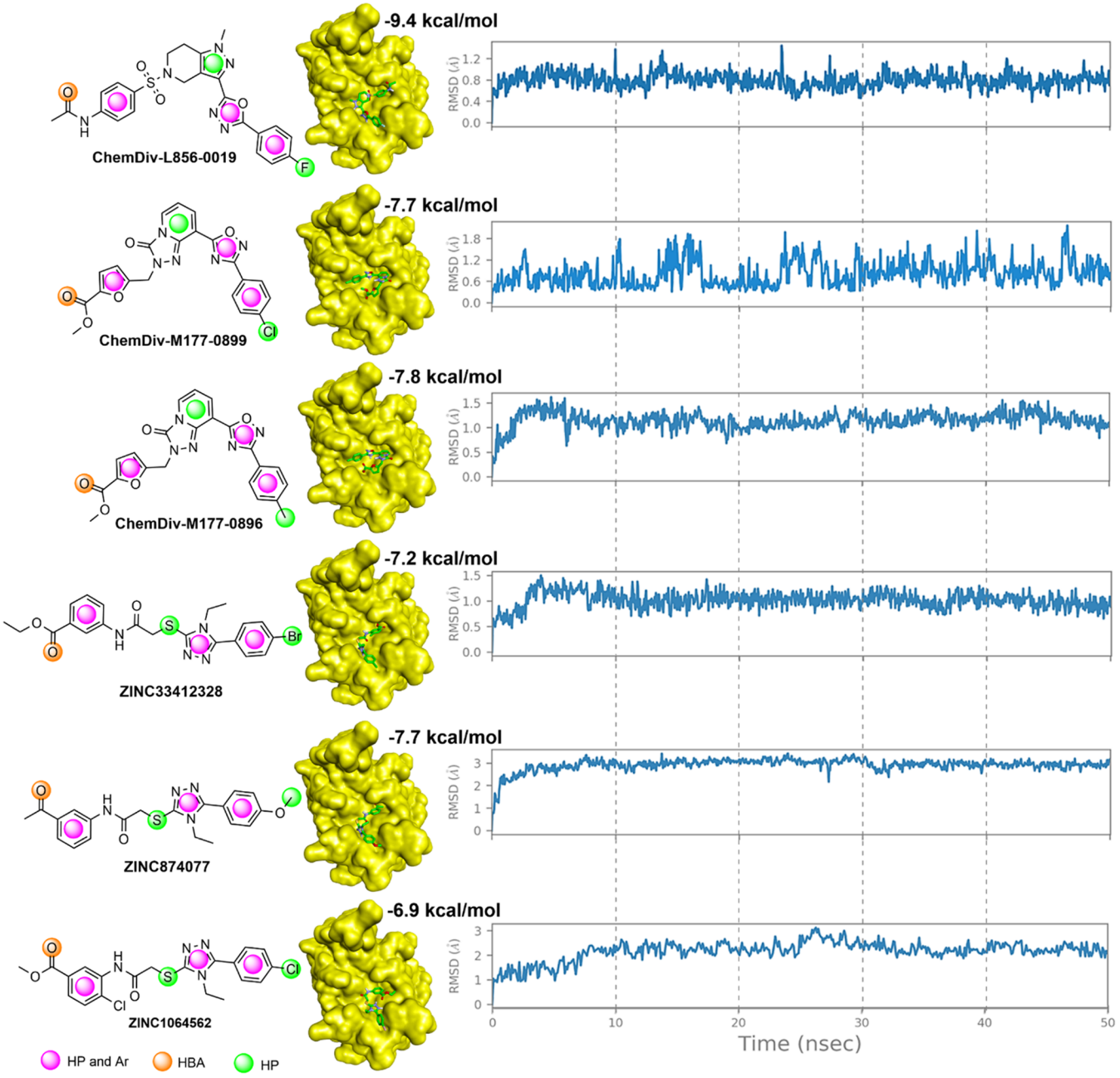

Figure 8. Redocking protocol and molecular dynamics of top three molecules virtual screened from ChemDiv and the ZINC database. HBA: hydrogen bond acceptor; HP: hydrophobic. Ar: aromatic ring.

the His51, Asp75, and Ser135 residues, resulting in a closed conformation of the oxyanion orifice.[27,46] The inhibitor binding caused a change from the active to inactive state in the catalytic triad of the NS3 protease. However, **9b** binding did not further induce significant conformational changes of protease (Figure 5), and this proposed a noncompetitive inhibitor binding on the ZIKV protease.[27,46,47] The dynamic simulation for the NS2B-NS3 protease also revealed that compound **9b** binds closely to five key amino acids (His51, Asp75, Ser135, Ala132, and Tyr161) at the active site of this protease. Unfortunately, in this study, we were unable to test NS2B-NS3 protease inhibition *in vitro* for providing more biological data. However, in this report, we attempted to use molecular docking and dynamic protocols to confirm **9b** as a potential compound to target the NS2B-NS3 protease. This would provide insight into ZIKV inhibition of the analogues in the future.

From these ligand-protease interactions, we build the pharmacophore model from six different features using the Pharmit spectrum (one HBA feature, two HP features, and three features of both HP and AR). The arrangement of steric and electronic characteristics of the pharmacophore was necessary to guarantee the finest molecular interactions with the respective biological target or the discovery of new scaffolds binding the active site of the NS2B-NS3 protease. After pharmacophore-based virtual screening, 839 compounds that showed similarity to the pharmacophore model (RMSD values less than 1.0 Å) were selected (Figure 7). The top ten compounds were identified based on the pharmacophore model from two large databases, ZINC and ChemDiv (RMSD

https://doi.org/10.1021/acsomega.3c06612
ACS Omega 2023, 8, 48994−49008

< 0.4 Å) (Supporting Information, Table S2). These compounds completely embodied the pharmacological features of the model, thereby enabling them to tightly bind to NS2B-NS3, and exhibited the ability to inhibit ZIKV. In particular, the redocking and molecular dynamics simulations of the top three compounds from each database revealed a significant binding affinity and stability with the NS2B-NS3 protease (Figure 8). Rehman et al. (2023) generated a pharmacophore model based on a five-featured pharmacophore hypothesis.[48] The results identified three hit molecules as potential inhibitors of Zika NS2B-NS3 protease with binding free energies of −64.28, −55.15, and −50.16 kcal/mol, as predicted by Schrödinger's GLIDE module. However, no follow-up *in vitro* evaluations has been conducted to verify these findings. The ZIKV NS3 protease pharmacophore model was utilized for virtual screening, resulting in the identification of 14 potential antiviral candidates by Pathak et al. (2020).[49] Subsequently, these candidates were tested via *in vitro* assays, and the Food and Drug Administration (FDA)-approved drugs asunaprevir and simeprevir exhibited potent anti-ZIKV activities with EC_{50} values of 4.7 μM and 0.4 μM, respectively. Furthermore, both drugs were able to inhibit the viral protease, exhibiting IC_{50} values of 6.0 and 2.6 μM, respectively.

This study endeavors to shed new light on heterocyclic compounds with antiviral potential, paving the way for the future development of robust ZIKV inhibitors. Altogether, the study opens new investigation possibilities in the search for novel drugs composed of a pyrazolo[3,4-*d*]pyridazine-7-one core to combat ZIKV. The *in vitro* antiviral activity of our synthesized compounds against ZIKV and their docking inhibition on ZIKV NS2B-NS3 were reported for the first time. High-throughput virtual screening could be used to screen for prospective ZIKV inhibitors based on the predicted pharmacophore model, and it will also be a subject of future reports. Furthermore, *in vitro* and *in vivo* studies on enzymes and animals were also needed to confirm its pharmacological effects and antiviral efficacy on ZIKV. ZIKV infection could dramatically affect fetal neural development, especially in neural stem cells. Thus, the antiviral activity of **9b** should be tested and validated in neural stem cells in the future.

4. CONCLUSION

Our study described a discovery of the anti-ZIKV potential of 16 pyrazolo[3,4-*d*]pyridazine-7-one compounds and advocated **9b** as an excellent candidate for further trials of ZIKV treatment. Compound **9b** was a novel structural feature that produced anti-ZIKV activity comparable to the positive control MPA. Through the brine shrimp lethality bioassay, **9b**, **10b**, **12**, **17a**, and **19a** showed acceptable toxicities with LD_{50} values in a range of 87.2−100.3 μg/mL. The docking dynamic simulation for the NS2B-NS3 protease also revealed that **9b** acts as a noncompetitive inhibitor and binds closely to five key amino acids (His51, Asp75, Ser135, Ala132, Tyr161) at the active site of this protease. Using the pharmacophore model of **9b**, a virtual screening was conducted to identify the top ZIKV inhibitors. Subsequently, molecular dynamics simulations were employed to evaluate the stability and binding affinity of the top six selected compounds with the NS2B-NS3 protease. More studies on *in vitro* and *in vivo* models are needed to confirm their therapeutic applications.

5. MATERIALS AND METHODS

5.1. General Information. All reagents were purchased from commercial sources and used without further purification. Reactions were monitored by thin-layer chromatography (TLC) on 0.2 mm precoated silica gel 60 F254 plates (Merck), and compounds were visualized on TLC with UV light. The derivatives were synthesized and then purified by flash column chromatography using silica gel 45−63 μm (230−400 mesh) and 60 pore size. The NMR spectra were obtained from a Varian 300 MHz or Bruker 300 MHz spectrometer. The chemical shifts (δ) were reported in parts per million (ppm) relative to tetramethylsilane (TMS) or the internal solvent signal of deuterated solvents. Multiplicities were indicated by *s* (singlet), *d* (doublet), *t* (triplet), and *m* (multiplet).

5.2. Chemistry. *Experimental Procedure of Compounds 2a−b.* To a stirred solution of compound **1** (50 mmol, 1.0 equiv) in a mixture of cold H_2O/conc. HCl (1:1; 20 mL) at 0 °C was slowly added a solution of $NaNO_2$ (1.1 equiv) in H_2O (10 mL). The mixture was stirred for 1 h at 0−5 °C, which gave the intermediate diazonium salt **2**, and this compound was used without any further purification for the next reaction step.

Experimental Procedure of Compounds 4a−b. Then a stirred mixture of NaOAc (3.0 equiv) and compound **3** (1.1 equiv) in EtOH (150 mL) at 0 °C was added to the mentioned intermediate diazonium salt **2** portionwise. The mixture was stirred for 4 h and poured into 500 mL of water. The precipitate was filtered off, dried, and recrystallized from EtOH, giving compound **4**.

*Compound **4a**.* Yield: 94%. ^{1}H NMR (300 MHz, DMSO-d_6, δ ppm): 10.53 (*s*, 1H, −N*H*−), 7.37−7.28 (*m*, 4H, Ar*H*), 7.02−6.96 (*m*, 1H, Ar*H*), 4.32−4.24 (*m*, 2H, −OCH_2CH$_3$), 1.32−1.27 (*m*, 3H, −OCH$_2$CH_3).

Compound **4b**.

Yield: 54%. ^{1}H NMR (300 MHz, DMSO-d_6, δ ppm): 10.43 (*s*, 1H, −NH−), 7.30−6.91 (*m*, 2H, ArH), 6.94−6.91 (*m*, 2H, ArH), 4.31−4.26 (*m*, 2H, −OCH_2CH$_3$), 3.72 (*s*, 3H, −OCH$_3$), 1.31−1.26 (*m*, 3H, −OCH_2CH$_3$).

Experimental Procedure of Compound 6a−b. Compound **5**, acetylacetone (1.1 equiv), was added to a stirred solution of 21% NaOEt/EtOH (1.1 equiv; diluted with 15 mL of anhydrous EtOH). The mixture was stirred at rt for 7 h, and then the finely powder compound **4** (20 mmol, 1.0 equiv) was added after being stirred for 4 h.

*For Compound **6a**.* The mixture was quenched with water, extracted twice with EtOAc, washed with brine, concentrated, and purified by flash column chromatography (EtOAc/Hex, 1:4 to 1:3), which gave the desired product **6a** in 93% yield as a yellow oil. ^{1}H NMR (300 MHz, DMSO-d_6, δ ppm): 7.62−7.54 (*m*, 5H, Ar*H*), 4.38−4.30 (*m*, 2H, −OCH_2CH$_3$), 2.47 (*s*, 3H, −CH_3), 2.37 (*s*, 3H, −COCH_3), 1.33−1.28 (*m*, 3H, −OCH_2CH$_3$).

*For Compound **6b**.* The mixture was added with cold water, and the precipitate was filtered off, dried, and recrystallized from EtOH, which gave desired product **6b** in 86% yield as a pale yellow solid. ^{1}H NMR (300 MHz, $CDCl_3$, δ ppm): 7.33−7.26 (*m*, 2H, ArH), 7.00−6.98 (*m*, 2H, ArH), 4.49−4.42 (*m*, 2H, −OCH_2CH$_3$), 3.87 (*s*, 3H, −OCH$_3$), 2.59 (*s*, 3H, −COCH$_3$), 2.38 (*s*, 3H, −COCH$_3$), 1.44−1.40 (*m*, 3H, −OCH_2CH$_3$).

https://doi.org/10.1021/acsomega.3c06612
ACS Omega 2023, 8, 48994−49008

Experimental Procedure of Compounds 7a−b. A mixture of compound **6** (5 mmol, 1.0 equiv) and excess hydrazine monohydrate in EtOH was refluxed for 2 h, then cooled, and kept at 0 °C for 20 min. The resulting precipitate was filtered off and dried to yield the desired product 7. Yield: 94% for **7a** and 95% for **7b**.

*Compound **7a**.* ^{1}H NMR (300 MHz, DMSO-d_6, δ ppm): 12.02 (*s*, 1H, −NH−), 7.63 (*s*, 5H, ArH), 2.61 (*s*, 3H, $-CH_3$), 2.49 (*s*, 3H, $-CH_3$). The molecular formula $C_{13}H_{12}N_4O$ was indicated by high-resolution electrospray ionization mass spectrometry (HR-ESI-MS) at *m*/*z* 241.1081 $[M + H]^+$ (Calcd for $[C_{13}H_{12}N_4OH]^+$, 241.1084).

*Compound **7b**.* ^{1}H NMR (300 MHz, DMSO-d_6, δ ppm): 11.96 (*s*, 1H, −NH−), 7.49 (*d*, *J* = 8.8 Hz, 2H, ArH), 7.12 (*d*, *J* = 7.3 Hz, 2H, ArH), 3.82 (*s*, 3H, $-OCH_3$), 2.54 (*s*, 3H, $-CH_3$), 2.45 (*s*, 3H, $-CH_3$). The molecular formula $C_{14}H_{14}N_4O_2$ was indicated by HR-ESI-MS at *m*/*z* 271.1189 [M + H]+ (Calcd for $[C_{14}H_{14}N_4O_2H]^+$, 271.1190).

Experimental Procedure of Compounds 9a−9b. To a stirred solution of compound **7** (1.0 mmol, 1.0 equiv) in DMF (anhydrous, 5 mL) at 0 °C was added NaH (60% in oil). The mixture was stirred for 30 min, and then **8** was added. After the starting material disappeared (about 30 min), the reaction mixture was quenched with cold water and extracted with EtOAc twice. The combined organic phase was washed with water twice and brine, dried with anhydrous Na_2SO_4, filtered, and concentrated. The resulting residue was purified by flash column chromatography (EtOAc/Hex, 1:1 to 2:1), which gave the desired products **9a** and **9b** as white solids. Yield: 93% for **9a** and 94% for **9b**.

*Compound **9a**.* ^{1}H NMR (300 MHz, $CDCl_3$, δ ppm): 8.26 (*s*, 1H, ArH), 8.13 (*d*, *J* = 8.1 Hz, 1H, ArH), 7.81 (*d*, *J* = 7.0 Hz, 1H, ArH), 7.54−7.46 (*m*, 6H, ArH), 5.46 (*s*, 2H, $-CH_2-$), 2.65 (*s*, 3H, $-CH_3$), 2.57 (*s*, 3H, $-CH_3$).

*Compound **9b**.* ^{1}H NMR (300 MHz, DMSO-d_6, δ ppm): 8.12−8.10 (*m*, 2H, ArH), 7.71 (*d*, *J* = 7.8 Hz, 1H, ArH), 7.61 (*t*, *J* = 8.1 Hz, 1H, ArH), 5.36 (*s*, 2H, $-CH_2-$), 3.82 (*s*, 3H, $-OCH_3$), 2.55 (*s*, 3H, $-CH_3$), 2.49 (*s*, 3H, $-CH_3$).

Experimental Procedure of Compounds 10a−b. To a stirred solution of compound **9** (0.5 mmol, 1.0 equiv) in EtOH (10 mL) at 80 °C was added $SnCl_2{\cdot}H_2O$ (5.0 equiv). The reaction mixture was stirred at 80 °C. After the starting material completely reacted (about 1 h), the reaction mixture was cooled to room temperature and neutralized with saturated $NaHCO_3$ solution at 0 °C, and the resulting mixture was filtered through a diatomaceous earth layer. The filtrate was extracted twice with EtOAc, washed with brine, dried with anhydrous Na_2SO_4, filtered, concentrated, and purified by flash column chromatography (EtOAc/Hex, 4:1 to 5:1), which gave the desired products **3a−b** as white solids. Yield: 75% for **10a** and 94% for **10b**.

*Compound **10a**.* ^{1}H NMR (300 MHz, DMSO-d_6, δ ppm): 7.60 (*s*, 5H, ArH), 6.90 (*t*, *J* = 7.6 Hz, 1H, ArH), 6.42−6.37 (*m*, 3H, ArH), 5.06 (*s*, 2H, $-CH_2-$), 5.00 (*s*, 2H, $-NH_2$), 2.59 (*s*, 3H, $-CH_3$), 2.58 (*s*, 3H, $-CH_3$).

*Compound **10b**.* ^{1}H NMR (300 MHz, DMSO-d_6, δ ppm): 7.52−7.48 (*m*, 2H, ArH), 7.15−7.11 (*m*, 2H, ArH), 6.90 (*t*, *J* = 7.7 Hz, 1H, ArH), 6.40−6.36 (*m*, 3H, ArH), 5.05 (*s*, 2H, $-CH_2-$), 5.06 (*s*, 2H, $-CH_2-$), 5.00 (*s*, 2H, $-NH_2$), 3.82 (*s*, 3H, $-OCH_3$), 2.55 (*s*, 3H, $-CH_3$), 2.46 (*s*, 3H, $-CH_3$).

Experimental Procedure of Compounds 11−14. To a stirred solution of compound **10** (0.2 mmol, 1.0 equiv) in DCM (5 mL) at 0 °C was added Et_3N (3.0 equiv). Then acyl chlorides, CH_3COCl or PhCOCl, (1.1 equiv) were added dropwise. The reaction mixture was stirred at 0 °C. After the starting material disappeared (30 min), the reaction mixture was added to cold water, extracted twice with DCM, washed with brine, dried with anhydrous Na_2SO_4, filtered, concentrated, and purified by flash column chromatography (EtOAc/Hex, 4:1 to 5:1), which gave the desired products **11** to **14** as white solids. Yield: 79 to 87%.

*Compound **11**.* ^{1}H NMR (300 MHz, DMSO-d_6, δ ppm): 9.88 (*s*, 1H, −NH−), 7.60 (*s*, 5H, ArH), 7.56−7.50 (*m*, 1H, ArH), 7.37 (*s*, 1H, ArH), 7.20 (*t*, *J* = 7.9 Hz, 1H, ArH), 6.92 (*d*, *J* = 7.6 Hz, 1H, ArH), 5.18 (*s*, 2H, $-CH_2-$), 2.58 (*s*, 3H, $-CH_3$), 2.49 (*s*, 3H, $-CH_3$), 1.96 (*s*, 3H, $-COCH_3$). The molecular formula $C_{22}H_{21}N_5O_2$ was indicated by HR-ESI-MS at *m*/*z* 388.1772 $[M + H]^+$ (Calcd for $[C_{22}H_{21}N_5O_2H]^+$, 388.1768).

*Compound **12**.* ^{1}H NMR (300 MHz, DMSO-d_6, δ ppm): 10.22 (*s*, 1H, −NH−), 7.95−7.89 (*m*, 2H, ArH), 7.71 (*d*, *J* = 8.1 Hz, 1H, ArH), 7.64−7.44 (*m*, 9H, ArH), 7.30−7.25 (*m*, 1H, ArH), 7.01 (*d*, *J* = 7.6 Hz, 1H, >CH−), 5.23 (*s*, 2H, $-CH_2-$), 2.59 (*s*, 3H, $-CH_3$), 2.50 (*s*, 3H, $-CH_3$). The molecular formula $C_{27}H_{23}N_5O_2$ was indicated by HR-ESI-MS at *m*/*z* 450.1932 $[M + H]^+$ (Calcd for $[C_{27}H_{23}N_5O_2H]^+$, 450.1925).

*Compound **13**.* ^{1}H NMR (300 MHz, DMSO-d_6, δ ppm): 9.89 (*s*, 1H, −NH−), 7.58−7.52 (*m*, 3H, ArH), 7.41 (*s*, 1H, ArH), 7.23 (*t*, *J* = 7.8 Hz, 1H, ArH), 7.17 (*d*, *J* = 8.5 Hz, 2H, ArH), 6.96 (*d*, *J* = 7.5 Hz, 1H, ArH), 5.21 (*s*, 2H, $-CH_2-$), 3.87 (*s*, 3H, $-OCH_3$), 2.59 (*s*, 3H, $-CH_3$), 2.50 (*s*, 3H, $-CH_3$), 2.00 (*s*, 3H, $-COCH_3$). The molecular formula $C_{23}H_{23}N_5O_3$ was indicated by HR-ESI-MS at *m*/*z* 418.1885 $[M + H]^+$ (Calcd for $[C_{23}H_{23}N_5O_3H]^+$, 418.1874).

Compound **14**: ^{1}H NMR (300 MHz, DMSO-d_6, δ ppm): 10.24 (*s*, 1H, −NH−), 7.93 (*d*, *J* = 7.4 Hz, 2H, ArH), 7.75 (*d*, *J* = 8.2 Hz, 1H, ArH), 7.66 (*s*, 1H, ArH), 7.60−7.48 (*m*, 5H, ArH), 7.31 (*t*, *J* = 7.9 Hz, 1H, ArH), 7.16 (*d*, *J* = 8.7 Hz, 2H, ArH), 7.04 (*d*, *J* = 7.6 Hz, 1H, ArH), 5.26 (*s*, 2H, $-CH_2-$), 3.86 (*s*, 3H, $-OCH_3$), 2.59 (*s*, 3H, $-CH_3$), 2.53 (*s*, 3H, $-CH_3$). The molecular formula $C_{28}H_{25}N_5O_3$ was indicated by HR-ESI-MS at *m*/*z* 480.2034 $[M + H]^+$ (Calcd for $[C_{28}H_{25}N_5O_3H]^+$, 480.2030).

Experimental Procedure of Compounds 17a−b. CuI (1.5 equiv) was added to a degassed mixture of compound **7** (1.0 mmol, 1.0 equiv), **15** (2.0 equiv), ligand **16** (0.15 equiv), and K_2CO_3 (1.5 equiv) in DMSO (anhydrous, 10 mL). The mixture was stirred at 150 °C under microwave conditions for 20 min. Then the reaction was quenched with cold water and added with EtOAc. The resulting suspension was filtered with a diatomaceous earth pad and washed several times with EtOAc. The organic phase was extracted twice with EtOAc, the combined EtOAc was washed 3 times with water, dried with Na_2SO_4, filtered, concentrated, and purified by flash column chromatography (EtOAc−Hex, 1:1 to 2:1), which gave the desired products **17a−b** as white solids. Yield: 55% for **17a** and 60% for **17b**.

*Compound **17a**.* ^{1}H NMR (300 MHz, DMSO-d_6, δ (ppm): 8.16−8.09 (*m*, 1H, ArH), 7.94 (*d*, *J* = 7.7 Hz, 1H, ArH), 7.86 (*d*, *J* = 8.0 Hz, 1H, ArH), 7.63 (*m*, 6H, ArH), 3.86 (*s*, 3H, $-COCH_3$), 2.63 (*s*, 3H, $-CH_3$), 2.56 (*s*, 3H, $-CH_3$).

*Compound **17b**.* ^{1}H NMR (300 MHz, DMSO-d_6, δ ppm): 8.14 (*t*, *J* = 1.9 Hz, 1H), 7.96−7.93 (*m*, 1H, ArH), 7.89−7.86 (*m*, 1H, ArH), 7.64 (*t*, *J* = 7.9 Hz, 1H, ArH), 7.57−7.53 (*m*, 2H, ArH), 7.19−7.13 (*m*, 2H, ArH), 3.88 (*s*, 3H, $-OCH_3$),

https://doi.org/10.1021/acsomega.3c06612
ACS Omega 2023, 8, 48994−49008

3.85 (*s*, 3H, $-COCH_3$), 2.61 (*s*, 3H, $-CH_3$), 2.56 (*s*, 3H, $-CH_3$).

Experimental Procedure of Compounds 18a–b. To a stirred solution of compound **17** (0.5 mmol, 1.0 equiv) in a mixture of tetrahydrofuran (THF)-MeOH (1:1, 10 mL) was added a solution of 1.0 M $LiOH/H_2O$ (excess). The reaction mixture was stirred at room temperature overnight. After the starting material disappeared, the mixture was concentrated to completely evaporate the solvents under a vacuum system. The resulting residue was acidified with 1.0 M HCl (aq) solution, then extracted twice with EtOAc, washed with brine, dried with Na_2SO_4, filtered, concentrated, and recrystallized, which gave the desired product **18a-b** as white solids. Yield: 90% for **18a** and 87% for **18b**.

Compound 18a. ^{1}H NMR (300 MHz, DMSO-d_6, δ ppm): 13.17 (*br*, 1H, −COOH), 8.13−8.09 (*m*, 1H, ArH), 7.93 (*d*, *J* = 7.6 Hz, 1H, ArH), 7.83 (*d*, *J* = 7.9 Hz, 1H, ArH), 7.69−7.57 (*m*, 6H, ArH), 2.65 (*s*, 3H, $-CH_3$), 2.58 (*s*, 3H, $-CH_3$).

Compound 18b. ^{1}H NMR (300 MHz, DMSO-d_6, δ ppm): 13.17 (*s*, 1H, −COOH), 8.13 (*s*, 1H, ArH), 7.95 (*d*, *J* = 7.7 Hz, 1H, ArH), 7.85 (*d*, *J* = 7.9 Hz, 1H, ArH), 7.64 (*d*, *J* = 7.9 Hz, 1H, ArH), 7.59−7.55 (*m*, 2H, ArH), 7.18 (*d*, *J* = 8.4 Hz, 2H, ArH), 3.87 (*s*, 3H, $-OCH_3$), 2.63 (*s*, 3H, $-CH_3$), 2.58 (*s*, 3H, $-CH_3$).

Experimental Procedure of Compounds 19a–b. To a stirred solution of compound **18** (0.5 mmol, 1.0 equiv), hydroxybenzotriazole (HOBT) (1.3 equiv) and EDC·HCl (1.3 equiv) in DMF (anhydrous, 5 mL) was added isopropylamine (excess). The mixture was stirred at room temperature to 50 °C overnight. After the starting material disappeared, the reaction product was added to cold water, extracted twice with EtOAc, washed twice with water, dried with Na_2SO_4, filtered, concentrated, and purified by flash column chromatography (EtOAc−Hex, 4:1 to EtOAc), which gave the desired product **19a-b** as white solids. Yield: 27% for **19a** and 36% for **19b**.

Compound 19a. ^{1}H NMR (300 MHz, DMSO-d_6, δ ppm): 8.33 (*d*, *J* = 7.8 Hz, 1H, ArH), 8.02 (*d*, *J* = 2.5 Hz, 1H, ArH), 7.88 (*d*, *J* = 7.7 Hz, 1H, ArH), 7.71−7.66 (*m*, 6H, ArH (5H), and −NH−(1H)), 7.57 (*t*, *J* = 7.8 Hz, 1H, ArH), 4.18−4.05 (*m*, 1H, $-NH-CH-(CH_3)_2$), 2.66 (*s*, 3H, $-CH_3$), 2.60 (*s*, 3H, $-CH_3$), 1.18 (*d*, *J* = 6.5 Hz, 6H, $-CH-(CH_3)_2$).

Compound 19b. ^{1}H NMR (300 MHz, DMSO-d_6, δ ppm): 8.33 (*d*, *J* = 7.7 Hz, 1H, ArH), 8.02 (*s*, 1H, ArH), 7.88 (*d*, *J* = 7.7 Hz, 1H, ArH), 7.69 (*d*, *J* = 8.0 Hz, 1H, ArH), 7.59−7.54 (*m*, 3H, ArH (2H), and −NH−(1H)), 7.19 (*d*, *J* = 8.4 Hz, 2H, ArH), 4.18−4.07 (*m*, 1H, $-NH-CH-(CH_3)_2$), 3.88 (*s*, 3H, $-OCH_3$), 2.64 (*s*, 3H, $-CH_3$), 2.59 (*s*, 3H, $-CH_3$), 1.18 (*d*, *J* = 6.4 Hz, 6H, $-CH-(CH_3)_2$).

5.3. Evaluation of Anti-ZIKV Activity. The experimental method against Zika virus was similar to that previously published.[3,4] Vero cells (ATCC, Manassas, USA) were cultured in Dulbecco's Modified Eagle's Medium (DMEM), 10% fetal bovine serum (FBS), 1% (penicillin and streptomycin), and 2 mM L-glutamine. Zika virus (MR766 Africa lineage, ATCC, USA, VR-1838) inoculated Aedes albopictus mosquito cells, clone C6/36. The culture was carried out for 14 days in EMEM, 1% FBS, 1% penicillin, and streptomycin, and then viral passages were kept at −80 °C for the experiments. Cells were pretreated with the test compounds at ten concentrations, then cells were infected (added 5 μL of ZIKV inoculum for each well) and continued to be incubated for 24 h. After 24 h, the cells were analyzed by immunofluorescence assay (should fix paraformaldehyde at 4%). Mycophenolate acid was used as a positive control in this study. The EC_{50} and CC_{50} values were calculated using Prism v7.0 software. The antiviral activity of tested compounds was evaluated by a 10-point DRC analysis in triplicate.

5.4. Brine Shrimp Lethality Bioassay. The brine shrimp lethality bioassay was performed similar to that previously published by Mayer et al.[32] First, the compounds were dissolved in small amounts of dimethyl sulfoxide (DMSO; Sigma, MA, USA), then serially diluted in simulated seawater to solutions of various concentrations (500, 250, 125, 62, 31, and 16 μg/mL). Second, randomly aspirate 20−35 naupliis into 5 mL of solution corresponding to each concentration. After 24 h, the number of surviving nauplii in each vial was counted and the brine shrimp's lethality percentage was calculated. Finally, the LD_{50} values were determined by probit analysis. The procedures were independently repeated three times.

5.5. Docking Studies. All ligands were performed with the aid of the Gaussian 09 program.[50] The geometries were fully optimized, making use of functional B3LYP in conjunction with the 6-31G(d,p) basis set for carbon and hydrogen atoms for compounds. The crystal structure of NS2B-NS3 in complex with a benzimidazol-1-ylmethanol inhibitor (PDB code: 5H4I) was retrieved from the Research Collaboratory for Structural Bioinformatics (RCSB).[27] All water molecules and small molecules were deleted by the Discovery Studio Visualizer. Autodock Tool version 4.2.6 was also used in the docking studies.[49] Grid box parameters were set to cover all of the residues around the active site. More specifically, it was centered on the ligand and comprised 60 × 60 × 60 points with 0.375 Å in spacing. The Lamarckian Genetic Algorithm was used to explore the best conformational space for the ligand, with 100 docking runs for each ligand. The maximum numbers of generation and evaluation were set at 27,000 and 50,000,000, respectively. Other parameters were set as default. After the docking process was completed, 100 conformations of the ligands in complex with the receptor were obtained and ranked based on binding energy.

5.6. Molecular Dynamic and Pharmacophore Model. All calculations were performed with the Desmond package 2018−4 (academic license). The protein−ligand docked complex was solvated with the single-point charge water model, and the overall charge of the system was neutralized. The parameters were set by default by the software. The simulation system was relaxed by constant NPT ensemble conditions to generate simulation data for postsimulation analyses. The full system contained 24118 atoms, and the temperature value was defined as 300 K and stable atmospheric pressure (1 atm). Pharmacophore model using Pharmit online (https://pharmit.csb.pitt.edu/search.html).[28]

■ ASSOCIATED CONTENT

Supporting Information

The Supporting Information is available free of charge at https://pubs.acs.org/doi/10.1021/acsomega.3c06612.

Spectral data (^{1}H NMR, HRMS spectra) and HPLC/GC-FID chromatograms for all compounds (Figures S1−S27); Biological assay data for all compounds (Table S1 and Figure S28); Molecular docking and pharmacophore model (Table S2 and Figures S29−S30) (PDF)

https://doi.org/10.1021/acsomega.3c06612
ACS Omega 2023, 8, 48994−49008

AUTHOR INFORMATION

Corresponding Authors

Cuong Quoc Nguyen − *Department of Chemistry, College of Natural Sciences, Can Tho University, Can Tho 94000, Vietnam; Analytical Techniques Lab (1.16-AT Department of Chemistry L), CTU High-tech Building, Can Tho University, Can Tho 94000, Vietnam;* orcid.org/0000-0002-5641-5040; Email: ncquoc99@gmail.com

Quang Le Dang − *Institute for Tropical Technology, Vietnam Academy of Science and Technology, Hanoi 10072, Vietnam; Graduate University of Science and Technology, Vietnam Academy of Science and Technology, Hanoi 10072, Vietnam;* orcid.org/0000-0001-7203-8081; Email: ldquang@itt.vast.vn, ledangquang2011@gmail.com

Hong Phuong Nguyen − *Department of Pediatrics, Indiana University School of Medicine, Indianapolis 46202 Indiana, United States*; Email: nguyeho@iu.edu, phuong.hn.jcb@gmail.com

Authors

Quang De Tran − *Department of Chemistry, College of Natural Sciences, Can Tho University, Can Tho 94000, Vietnam; Analytical Techniques Lab (1.16-AT Department of Chemistry L), CTU High-tech Building, Can Tho University, Can Tho 94000, Vietnam;* orcid.org/0000-0002-5381-0686

Thi Hong Minh Nguyen − *Department of Life Science, University of Science and Technology of Ha Noi, Vietnam Academy of Science and Technology, Ha Noi 10072, Vietnam*

Bui Thi Buu Hue − *Department of Chemistry, College of Natural Sciences, Can Tho University, Can Tho 94000, Vietnam*

Minh Uyen Thi Le − *Department of Surgery, Division of Transplant Surgery, Indiana University School of Medicine, Indianapolis 46202 Indiana, United States*

Nguyen Trong Tuan − *Department of Chemistry, College of Natural Sciences, Can Tho University, Can Tho 94000, Vietnam*

Nguyen Quoc Chau Thanh − *Department of Chemistry, College of Natural Sciences, Can Tho University, Can Tho 94000, Vietnam*

Tran Thanh Men − *Department of Biology, College of Natural Sciences, Can Tho University, Can Tho 94000, Vietnam*

Pham Minh Quan − *Graduate University of Science and Technology, Vietnam Academy of Science and Technology, Hanoi 10072, Vietnam; Institute of Natural Products Chemistry, Vietnam Academy of Science and Technology, Ha Noi 10072, Vietnam*

Nguyen Duy Tuan − *Nam Can Tho University, Can Tho 94000, Vietnam*

Thai Thi Cam − *Nam Can Tho University, Can Tho 94000, Vietnam*

Nguyen Thi Thu Thuy − *National Institute of Hygiene and Epidemiology, Hai Ba Trung, Ha Noi 10000, Vietnam*

Vu Thi Bich Hau − *National Institute of Hygiene and Epidemiology, Hai Ba Trung, Ha Noi 10000, Vietnam*

Tran Duy Binh − *Department of Biology, College of Natural Sciences, Can Tho University, Can Tho 94000, Vietnam*

Complete contact information is available at: https://pubs.acs.org/10.1021/acsomega.3c06612

Author Contributions

All authors have given approval to the final version of the manuscript.

Notes

The authors declare no competing financial interest.

ACKNOWLEDGMENTS

The authors would like to thank Can Tho University for its facilities support. This work was supported by the Ministry of Education and Training of Vietnam under grant No. B2019-TCT-37 (TCT-05) and Scientific research project of Can Tho University (T2023-19).

REFERENCES

(1) Pires, L. C.; Dantas, L. R.; Witkin, S. S.; Bertozzi, A. P. A. P.; Dezena, R. de C. A. B.; Rodrigues, M. M. D.; Gazeta, R. E.; Passos, S. D. Knowledge of Zika virus transmission and its prevention among high-risk pregnant women in Brazil. *Viruses* **2021**, *13*, 242.

(2) Siddique, R.; Liu, Y.; Nabi, G.; Sajjad, W.; Xue, M.; Khan, S. Zika virus potentiates the development of neurological defects and microcephaly: Challenges and control strategies. *Front. Neurol.* **2019**, *10*, 219.

(3) Hue, B. T. B.; Nguyen, P. H.; De, T. Q.; Van Hieu, M.; Jo, E.; Van Tuan, N.; Thoa, T. T.; Anh, L. D.; Son, N. H.; La Duc Thanh, D.; Dupont-Rouzeyrol, M.; Grailhe, R.; Windisch, M. P. Benzimidazole derivatives as novel zika virus inhibitors. *ChemMedChem.* **2020**, *15*, 1453.

(4) Nguyen, C. Q.; Nguyen, T. H. M.; Nguyen, T. T. T.; Bui, T. B. H.; Nguyen, T. T.; Huynh, N. T.; Le, T. D.; Nguyen, T. M. P.; Nguyen, D. T.; Nguyen, M. T.; Pham, M. Q.; Tran, Q. D.; Nguyen, H. P. Designs, synthesis, docking studies, and biological evaluation of novel berberine derivatives targeting zika virus. *J. Chem.* **2021**, *2021*, No. e5567111.

(5) Nagawade, R. R.; Khanna, V. V.; Bhagwat, S. S.; Shinde, D. B. Synthesis of new series of 1-aryl-1, 4-dihydro-4-oxo-6-methyl pyridazine-3-carboxylic acid as potential antibacterial agents. *Eur. J. Med. Chem.* **2005**, *40*, 1325.

(6) Ellis, G. P. *Synthesis of Fused Heterocycles;* Part 1; John Wiley & Sons, 2009; Vol. *47*.

(7) Asif, M. Pharmacologically potentials of hydrazonone containing compounds: A promising scaffold. *Int. J. Adv. Chem.* **2014**, *2*, 85.

(8) Tang, J.; Wang, B.; Wu, T.; Wan, J.; Tu, Z.; Njire, M.; Wan, B.; Franzblauc, S. G.; Zhang, T.; Lu, X.; Ding, K. Design, synthesis, and biological evaluation of pyrazolo [1, 5-a] pyridine-3-carboxamides as novel antitubercular agents. *ACS Med. Chem. Lett.* **2015**, *6*, 814.

(9) Abdelriheem, N.; Zaki, Y.; Abdelhamid, A. Synthesis of some new pyrazolo [1, 5-a] pyrimidine, pyrazolo [5, 1-c] triazine, 1,3,4-thiadiazole and pyridine derivatives containing 1,2,3-triazole moiety. *Chem. Cent. J.* **2017**, *11*, 1.

(10) Kumar, S.; Gupta, S.; Abadi, L. F.; Gaikwad, S.; Desai, D.; Bhutani, K. K. S.; Kulkarni, S.; Singh, I. P. Synthesis and in-vitro anti-HIV-1 evaluation of novel pyrazolo[4,3-c]pyridin-4-one derivatives. *Eur. J. Med. Chem.* **2019**, *183*, 111714.

(11) Arias-Gómez, A.; Godoy, A.; Portilla, J. Functional Pyrazolo-[1,5-*a*]pyrimidines: Current Approaches in Synthetic Transformations and Uses As an Antitumor Scaffold. *Molecules* **2021**, *26*, 2708.

(12) Akbas, E.; Berber, I. Antibacterial and antifungal activities of new pyrazolo[3,4-*d*]pyridazin derivatives. *Eur. J. Med. Chem.* **2005**, *40*, 401.

(13) Braña, M. F.; Cacho, M.; García, M. L.; Mayoral, E. P.; López, B.; de Pascual-Teresa, B.; Ramos, A.; Acero, N.; Llinares, F.; Muñoz-Mingarro, D.; Lozach, O.; Meijer, L. Pyrazolo [3,4-*c*] pyridazines as novel and selective inhibitors of cyclin-dependent kinases. *J. Med. Chem.* **2005**, *48*, 6843.

(14) Tewari, A. K.; Mishra, A. Synthesis and anti-inflammatory activities of N4, N5-disubstituted-3-methyl-1H-pyrazolo [3, 4-c] pyridazines. *Bioorg. Med. Chem.* **2001**, *9*, 715.

https://doi.org/10.1021/acsomega.3c06612
ACS Omega 2023, 8, 48994−49008

(15) Tavares, F. X.; Boucheron, J. A.; Dickerson, S. H.; Griffin, R. J.; Preugschat, F.; Thomson, S. A.; Wang, T. Y.; Zhou, H.-Q. N-Phenyl-4-pyrazolo [1, 5-*b*] pyridazin-3-ylpyrimidin-2-amines as potent and selective inhibitors of glycogen synthase kinase 3 with good cellular efficacy. *J. Med. Chem.* **2004**, *47*, 4716.
(16) Ghareb, N.; Elshihawy, H. A.; Abdel-Daim, M. M.; Helal, M. A. Novel pyrazoles and pyrazolo [1,2-*a*] pyridazines as selective COX-2 inhibitors; Ultrasound-assisted synthesis, biological evaluation, and DFT calculations. *Bioor. Med. Chem. Lett.* **2017**, *27*, 2377.
(17) Wang, Y.; Dai, Y.; Wu, X.; Li, F.; Liu, B.; Li, C.; Liu, Q.; Zhou, Y.; Wang, B.; Zhu, M.; Cui, R.; Tan, X.; Xiong, Z.; Liu, J.; Tan, M.; Xu, Y.; Geng, M.; Jiang, H.; Liu, H.; Ai, J.; Zheng, M. Discovery and development of a series of pyrazolo [3, 4-d] pyridazinone compounds as the novel covalent fibroblast growth factor receptor inhibitors by the rational drug design. *J. Med. Chem.* **2019**, *62*, 7473.
(18) Jacomini, A. P.; Silva, M. J. V.; Silva, R. G. M.; Gonçalves, D. S.; Volpato, H.; Basso, E. A.; Paula, F. R.; Nakamura, C. V.; Sarragiotto, M. H.; Rosa, F. A. Synthesis and evaluation against Leishmania amazonensis of novel pyrazolo [3,4-*d*] pyridazinone-*N*-acylhydrazone-(bi) thiophene hybrids. *Eur. J. Med. Chem.* **2016**, *124*, 340.
(19) Bildirici, İ.; Şener, A.; Atalan, E.; Battal, A.; Genç, H. Synthesis and antibacterial activity of 4-benzoyl-1-(4-carboxy-phenyl)-5-phenyl-1 H-pyrazole-3-carboxylic acid and derivatives. *Med. Chem. Res.* **2009**, *18*, 327.
(20) Fayed, A.; Al-Harbi, N.; Amr, A. E.-G.; Kalmoush, A.; Shadid, K.; Flefel, E. Synthesis, reactions, and pharmacological evaluations of some novel pyridazolopyridiazine candidates. *J. Heterocycl. Chem.* **2014**, *51*, 1770.
(21) Deeb, A.; Abdelgawad, A. A. M. Utility of 3-amino-1 H-pyrazolo [3, 4-c] pyridazine in heterocyclic synthesis. *Chem. Heterocycl. Compd.* **2015**, *51*, 785.
(22) Ghorbani-Vaghei, R.; Mahmoodi, J.; Maghbooli, Y. Preparation and characterization of nanomagnetic piperidinium benzene-1, 3-disulfonate ionic liquid as a novel, green and heterogeneous catalyst and its use in the synthesis of 1H-pyrazolo [1,2-*b*] phthalazine-5, 10-diones and 1H-pyrazolo [1,2-a] pyridazine-5, 8-diones under solvent-free conditions. *Appl. Organomet. Chem.* **2017**, *31*, No. e3717.
(23) Çetin, A.; Bildirici, İ. A study on synthesis and antimicrobial activity of 4-acyl-pyrazoles. *J. Saudi Chem. Soc.* **2018**, *22*, 279.
(24) Kumbar, M. N.; Shaikh, S. K. J.; Kamble, R. R.; Bayannavar, P. K.; Kamble, A. A.; Hunnur, R. K. Serendipitous formation of 2H-pyrazolo [3, 4-d] pyridazin-7 (6H)-ones from 3-arylsydnones. *ACS Omega* **2019**, *4*, 4955.
(25) Mady, M. F.; Saleh, T. S.; El-Kateb, A. A.; Abd El-Rahman, N. M.; Abd El-Moez, S. I. Microwave-assisted synthesis of novel pyrazole and pyrazolo [3, 4-d] pyridazine derivatives incorporating diaryl sulfone moiety as potential antimicrobial agents. *Res. Chem. Intermed.* **2016**, *42*, 753.
(26) Jacomini, A. P.; da Silva, M. J. V.; Poletto, J.; Ribeiro, G. M.; Yokoyama, J. T. C.; Bidóia, D. L.; Paula, F. R.; Nakamura, C. V.; Sarragiotto, M. H.; Rosa, F. A. Potential antileishmanial activity of 4-N-acylhydrazone pyrazolo [3,4-d] pyridazin-7-ones: Synthesis, in vitro biological evaluations and computational studies. *J. Braz. Chem. Soc.* **2018**, *29*, 2657.
(27) Zhang, Z.; Li, Y.; Loh, Y. R.; Phoo, W. W.; Hung, A. W.; Kang, C.; Luo, D. Crystal structure of unlinked NS2B-NS3 protease from Zika virus. *Science* **2016**, *354*, 1597.
(28) Sunseri, J.; Koes, D. R. Pharmit: interactive exploration of chemical space. *Nucleic Acids Res.* **2016**, *44*, W442.
(29) Kadow, J. F.; Pracitto, R. United States, US8324212B2, 2012.
(30) Elfiky, A. A. Zika viral polymerase inhibition using anti-HCV drugs both in market and under clinical trials. *J. Med. Virol.* **2016**, *88*, 2044.
(31) Hamdy, N. A.; El-Senousy, W. M. Synthesis and antiviral evalution of some novel pyrazoles and pyrazolo[3,4-d]pyridazines bearing 5,6,7,8-tetrahydronaphthalene. *Acta Pol. Pharm.* **2012**, *70*, 99−110.
(32) Meyer, B. N.; Ferrigni, N. R.; Putnam, J. E.; Jacobsen, L. B.; Nichols, D. E.; McLaughlin, J. L. Brine shrimp: a convenient general bioassay for active plant constituents. *Planta Med.* **1982**, *45*, 31.
(33) Ali, M. I.; Liton, M. A. K. Cytotoxicity, 2D-and 3D-QSAR study of some halogen containing hydroxy and amino substituted aromatic compounds. *World J. Org. Chem.* **2015**, *3* (1), 16−26.
(34) Rayees Ahmad, M.; Girija Sastry, V.; Bano, N.; Anwar, S. Synthesis of novel chalcone derivatives by conventional and microwave irradiation methods and their pharmacological activities. *Arabian J. Chem.* **2016**, *9*, S931.
(35) Definition of berberine chloride - NCI Drug Dictionary - NCI, https://www.cancer.gov/publications/dictionaries/cancer-drug/def/berberine-chloride, (accessed 2022-08-24).
(36) Berberine, https://go.drugbank.com/drugs/DB04115, (accessed 2022-08-24).
(37) Atropine, https://go.drugbank.com/drugs/DB00572, (accessed 24, 2022-08-24).
(38) Yadav, R.; Selvaraj, C.; Aarthy, M.; Kumar, P.; Kumar, A.; Singh, S. K.; Giri, R. Investigating into the molecular interactions of flavonoids targeting NS2B-NS3 protease from ZIKA virus through in-silico approaches. *J. Biomol. Struct. Dyn.* **2021**, *39*, 272.
(39) Choudhry, H.; Alzahrani, F. A.; Hassan, M. A.; Alghamdi, A.; Abdulaal, W. H.; Bakhrebah, M. A.; Zamzami, M. A.; Helmi, N.; Bokhari, F. F.; Zeyadi, M.; Baothman, O. A.; Kamal, M. A.; Warsi, M. K.; Ali, A.; Jarullah, B.; Jamal, M. S. Zika virus targeting by screening inhibitors against NS2B/NS3 protease. *Biomed. Res. Int.* **2019**, *2019*, No. e3947245.
(40) Wang, L.; Liang, R.; Gao, Y.; Li, Y.; Deng, X.; Xiang, R.; Zhang, Y.; Ying, T.; Jiang, S.; Yu, F. Development of small-molecule inhibitors against zika virus infection. *Front. Microbiol.* **2019**, *10*, 2725.
(41) Voss, S.; Nitsche, C. Inhibitors of the Zika virus protease NS2B-NS3. *Bioor. Med. Chem. Lett.* **2020**, *30*, 126965.
(42) Thirumoorthy, G.; Tarachand, S. P.; Nagella, P.; Veerappa Lakshmaiah, V. Identification of potential ZIKV NS2B-NS3 protease inhibitors from Andrographis paniculata: An in silico approach. *J. Biomol. Struct. Dyn.* **2022**, *40*, 11203.
(43) Coronado, M. A.; Eberle, R. J.; Bleffert, N.; Feuerstein, S.; Olivier, D. S.; de Moraes, F. R.; Willbold, D.; Arni, R. K. Zika virus NS2B/NS3 proteinase: A new target for an old drug-Suramin a lead compound for NS2B/NS3 proteinase inhibition. *Antivir. Res.* **2018**, *160*, 118.
(44) Wu, H.; Bock, S.; Snitko, M.; Berger, T.; Weidner, T.; Holloway, S.; Kanitz, M.; Diederich, W. E.; Steuber, H.; Walter, C.; Hofmann, D.; Weißbrich, B.; Spannaus, R.; Acosta, E. G.; Bartenschlager, R.; Engels, B.; Schirmeister, T.; Bodem, J. Novel dengue virus NS2B/NS3 protease inhibitors. *J. Bodem, Antimicrob. Agents Chemother.* **2015**, *59*, 1100.
(45) Rehman, H. M.; Sajjad, M.; Ali, M. A.; Gul, R.; Irfan, M.; Naveed, M.; Bhinder, M. A.; Ghani, M. U.; Hussain, N.; Said, A. S. A.; Al Haddad, A. H. I.; Saleem, M. Identification of NS2B-NS3 protease inhibitors for therapeutic application in zikv infection: A pharmacophore-based high-throughput virtual screening and MD simulations approaches. *Vaccines* **2023**, *11*, 131.
(46) Ren, J.; Lee, H.; Kotak, A.; Johnson, M. E. MD simulations reveal alternate conformations of the oxyanion hole in the Zika virus NS2B/NS3 protease. *Proteins: Struct. Funct. Bioinform.* **2020**, *88*, 345.
(47) de Paula Junior, V. F.; van Tilburg, M. F.; Morais, P. A.; Júnior, F. F. M.; Lima, E. G.; Oliveira, V. T. D. S.; Guedes, M. I. F.; Caetano, E. W. S.; Freire, V. N. Quantum biochemistry and MM-PBSA description of the ZIKV NS2B-NS3 protease: Insights into the binding interactions beyond the catalytic triad pocket. *Int. J. Mol. Sci.* **2022**, *23*, 10088.
(48) Pathak, N.; Kuo, Y.-P.; Chang, T.-Y.; Huang, C.-T.; Hung, H.-C.; Hsu, J. T.-A.; Yu, G.-Y.; Yang, J.-M. Zika virus NS3 protease pharmacophore anchor model and drug discovery. *Sci. Rep.* **2020**, *10*, 8929.
(49) Frisch, M.; Trucks, G.; Schlegel, H. B.; Scuseria, G. E.; Robb, M. A.; Cheeseman, J. R.; Scalmani, G.; Barone, V.; Mennucci, B. *Gaussian 09,* (Revision A.02); Gaussian Inc.: Wallingford, CT, 2016.

https://doi.org/10.1021/acsomega.3c06612
ACS Omega 2023, 8, 48994−49008

(50) Morris, G. M.; Goodsell, D. S.; Halliday, R. S.; Huey, R.; Hart, W. E.; Belew, R. K.; Olson, A. J. Automated docking using a Lamarckian genetic algorithm and an empirical binding free energy function. *J. Comput. Chem.* **1998**, *19*, 1639.

https://doi.org/10.1021/acsomega.3c06612
ACS Omega 2023, 8, 48994−49008